Ion Fluxes in Giant Excised Cardiac Membrane Patches Detected and Quantified with Ion-selective Microelectrodes

Tong Mook Kang,[1] Vladislav S. Markin,[2] and Donald W. Hilgemann[1]

[1]Departments of Physiology and [2]Anaesthesiology and Pain Management, The University of Texas Southwestern Medical Center at Dallas, Dallas, TX 75390

ABSTRACT We have used ion-selective electrodes (ISEs) to quantify ion fluxes across giant membrane patches by measuring and simulating ion gradients on both membrane sides. Experimental conditions are selected with low concentrations of the ions detected on the membrane side being monitored. For detection from the cytoplasmic (bath) side, the patch pipette is oscillated laterally in front of an ISE. For detection on the extracellular (pipette) side, ISEs are fabricated from flexible quartz capillary tubing (tip diameters, 2–3 microns), and an ISE is positioned carefully within the patch pipette with the tip at a controlled distance from the mouth of the patch pipette. Transport activity is then manipulated by solution changes on the cytoplasmic side. Ion fluxes can be quantified by simulating the ion gradients with appropriate diffusion models. For extracellular (intrapatch pipette) recordings, ion diffusion coefficients can be determined from the time courses of concentration changes. The sensitivity and utility of the methods are demonstrated with cardiac membrane patches by measuring (a) potassium fluxes via ion channels, valinomycin, and Na/K pumps; (b) calcium fluxes mediated by Na/Ca exchangers; (c) sodium fluxes mediated by gramicidin and Na/K pumps; and (d) proton fluxes mediated by an unknown electrogenic mechanism. The potassium flux-to-current ratio for the Na/K pump is approximately twice that determined for potassium channels and valinomycin, as expected for a 3Na/2K pump stoichiometery (i.e., 2K/charge moved). For valinomycin-mediated potassium currents and gramicidin-mediated sodium currents, the ion fluxes calculated from diffusion models are typically 10–15% smaller than expected from the membrane currents. As presently implemented, the ISE methods allow reliable detection of calcium and proton fluxes equivalent to monovalent cation currents <1 pA in magnitude, and they allow detection of sodium and potassium fluxes equivalent to <5 pA currents. The capability to monitor ion fluxes, independent of membrane currents, should facilitate studies of both electrogenic and electroneutral ion–coupled transporters in giant patches.

KEY WORDS: ion-selective electrodes • patch clamp • Na/K pump • Na/Ca exchange • proton transport

INTRODUCTION

For very good reasons, progress in understanding the function of ion transporters lags behind progress for ion channels. Voltage clamp methods allow detailed analysis of ion channel function, including ion permeation, channel gating, and channel regulation, often at the level of single channels (Hamill et al., 1981; Sigworth, 1986). The achievement of comparable functional studies for ion transporters is enormously more challenging, and at the same time ion transporter function is intrinsically much more complex. Multiple ion species are often moved by ion transporters, and minimal models of transporter function typically require several ion-dependent conformational changes (Läuger, 1987). Furthermore, ion transport can occur without generation of any membrane current, or with a complex relationship to membrane current. Certainly, progress in understanding the function and regulation of electroneutral ion transporters would benefit greatly from the development of improved methods to monitor ion transport. Electroneutral transporters of great importance in physiology and pathology include Na/H exchangers (Karmazyn et al., 1999; Karmazyn, 2001), anion exchangers (Kopito, 1990), proton-coupled monocarboxylate transporters (Bonen, 2001), and some Na/bicarbonate cotransporters (Boron, 2001; Soleimani and Burnham, 2001). Also, they include Na/K/Cl cotransporters (Haas and Forbush, 1998, 2000; Russell, 2000) and Na/Cl cotransporters (Hebert, 1998) that play central roles in epithelial salt transport, water transport, and cell volume regulation (Russell, 2000), and they include K/Cl cotransporters (Lauf and Adragna, 2000) that may importantly determine cytoplasmic chloride concentrations in neurons and thereby the effects of activating ligand-gated chloride channels (Hubner et al., 2001).

The measurement of transmembrane ion fluxes is one of the classical methodological problems of physiology, and numerous experimental techniques and ap-

Tong Mook Kang's present address is Department of Physiology, Sungkyunkwan University School of Medicine, Suwon 440-746, Korea.

Address correspondence to Donald W. Hilgemann, Department of Physiology University of Texas Southwestern Medical Center at Dallas, 5323 Harry Hines Boulevard Dallas, TX 75390-9040. Fax: (214) 648-8879; E-mail: donald.hilgemann@utsouthwestern.edu

proaches have been developed. They include isotope flux methods, ion-selective electrodes (ISEs),* and optical measurements using fluorescent dyes, usually using isolated cells or membrane vesicles (Stein, 1985). General problems encountered are that ion concentrations change during measurements, or cannot be controlled, time resolution is usually quite limited, and control of membrane potential in the presence of fluxes is often very limited. Particularly in whole-cell measurements, access to the cytoplasmic membrane side is usually very limited, thereby impairing control of ion concentrations and the ability to study exogenous regulatory factors (e.g., proteins).

One relatively new strategy, which motivated the present work, is the use of self-referenced ISEs to detect ion activity gradients that develop next to membranes during ion transport (Smith et al., 1994, 1999; Smith, 1995). Briefly, ISEs are moved in an oscillatory fashion (i.e., "vibrating probe") up to and away from a cell surface. Potential differences between the two positions then indicate the possible presence of an ion gradient caused by ion transport processes in the membrane. Using this approach, calcium, potassium, and proton fluxes have been characterized in a number of cell types, and in some cases an ion flux could be localized to specific cell domains (Smith and Trimarchi, 2001).

Given this success, a similar approach seemed promising to detect ion fluxes across giant membrane patches (Hilgemann, 1989; Hilgemann and Lu, 1998). Major advantages of the giant patch system for ion transporter studies include the following: (a) solution compositions can be controlled accurately on both membrane sides, (b) the inside-out patch configuration allows free access to the cytoplasmic side, and (c) membrane currents can be recorded from a large membrane area with fast membrane potential control. By placing the ISEs at either side of the excised patches, ion fluxes mediated by several transport systems might be detected. We describe here our initial experience with these methods to measure potassium, calcium, sodium, and proton fluxes generated by ion transporters present in cardiac surface membranes. We also describe strategies to calibrate results for both membrane sides and to test the accuracy of calibrations. Advantages and limitations of the methods are discussed.

MATERIALS AND METHODS

Cardiac Myocytes

Myocytes were isolated from guinea pig and mouse ventricles as described previously (Collins et al., 1992). In brief, guinea pigs or mice were killed by intraperitoneal injection of pentobarbital sodium (2 mg/g). After cessation of reflexes, hearts were rapidly removed and transferred to a Langendorff-type apparatus for retrograde perfusion at ~2 ml/gram/min. Collagenase (Liberase Blenzyme 4, ~0.1 mg/ml; Roche Diagnostic Corp.) was dissolved into a nominally calcium-free solution that contained (in mM): 140 NaCl, 4 KCl, 10 HEPES, 0.5 Na_2HPO_4, 2 taurine, 1 $MgCl_2$, and 15 glucose (pH 7.4 with NaOH). Hearts were perfused with enzymes for 15 min at 37°C, and digested tissue segments were placed in a "storage solution" containing (in mM): 140 KCl, 5 EGTA, 1 $MgCl_2$, 20 glucose, and 10 HEPES (pH 7.4 with KOH). Myocytes were stored at 4°C and were used in experiments after 6–48 h. Giant patches were formed on the large membrane blebs that develop on myocytes under these conditions (Hilgemann, 1989; Collins et al., 1992).

Patch Clamp

Membrane potential in all experiments described was 0 mV (Axopatch 1D), and signals were either acquired digitally or plotted directly onto chart paper (12 Hz response; Kipp and Zonen). In the latter case, figures were prepared from the data records after careful reproduction from scanned images. Leak currents were not subtracted, and all results presented are with patches at 34–36°C.

Ion-selective Microelectrodes

The ion-selective microelectrodes for the measurement of ion concentrations in the bath solution were fabricated from standard borosilicate glass tubing. The electrodes for measurements inside of the patch pipette were manufactured from flexible quartz capillary tubing (350 μm o.d./200 μm i.d./TSP200350; PolymicroTechnologies). The relatively small diameter and flexibility of this tubing allows easy placement of the electrodes within the patch pipette, whereby the electrode is threaded vertically through a polyethylene tube in the plexiglass pipette holder, which serves as guard when replacing patch pipettes. Generally, we followed published electrode fabrication protocols (Smith et al., 1999). Borosilicate glass electrodes (1.2 mm) without filament (cat. no. TW120–4, WPI) were pulled with a vertical puller (PP-83; Narishige), usually by a conventional double-pull protocol, giving tip diameters of 2–3 μm. The quartz tubes were cut about ~20-cm long and pulled by hand on a gas torch in the horizontal axis. The success rate in obtaining relatively constant shank lengths (<1 cm long) was >50% with experience. After pulling, ashes on the surface of the quartz electrodes were gently cleaned away with tissue. When the tip diameters were <2 μm, tips were beveled on the edge of a soft glass bead on the patch pipette microforge to give diameters of ~3 μm. Borosilicate and quartz electrodes were then placed upright in stainless steel or fine copper mesh racks, respectively, the racks were placed on a glass petri dish covered with a 1 liter silanized glass beaker, and the electrodes were baked in an oven at 200°C overnight or longer. Success rates for obtaining stable electrodes were higher for quartz electrodes when they were baked for at least 48 h. The dried electrodes were exposed in a vented hood to 0.05–0.1 ml of N,N-dimethyltrimethylsilylamine (cat. no. 41716; Fluka) for 30–40 min at 200°C by injecting the silane under the beaker through a syringe with bent needle. Surplus silane vapor was removed by opening the beaker for 30 s, and the silanized electrodes were then baked at 200°C overnight or more. The electrodes were stored in a dry dessicator or in the hot drying oven at 200°C until use.

In final preparation for use, the electrodes were back-filled with electrolyte solution containing 100 mM KCl (pH 7.0 with 5 mM HEPES) for potassium- and proton-selective electrodes, 100 mM $CaCl_2$ (pH 7.0 with 5 mM HEPES) for calcium-selective electrodes, 100 mM NaCl (pH 7.0 with 5 mM HEPES) for sodium-selective electrodes. The quartz electrodes were filled by applying pressure through a syringe that made a tight connection to a

Abbreviation used in this paper: ISE, ion-selective electrode.

thinner quartz tubing (150 μm o.d., cat. no. TSP075150; Polymicro Technologies) and could be inserted into the electrode. All electrolyte solutions were filtered (0.22 μm) before filling. A silanized pipette (a 1.2 mm o.d. of borosilicate electrode) was used to dispense the desired liquid ion-exchange resin (LIX). To do so, the microelectrode and the dispensing pipette were positioned in the same focal plane under a binocular compound microscope. The back-filled electrolyte solution was pushed forward to the tip using positive pressure through a polyethylene tube connected to a syringe. Upon touching the electrode tip to the surface of the ionophore cocktail, the ionophore flowed efficiently into the tip without any negative pressure. Column lengths were 50–150 μm for all ISEs employed in this study. The exact length of each column was measured under the microscope, and during experiments the column length was used as one means to calibrate distances between the patch pipette tip and the tip of the ISE.

Potassium ionophore I cocktail B (cat. no. 60398; Fluka), calcium ionophore I cocktail A (cat. no. 21048; Fluka), sodium ionophore I cocktail A (cat. no. 71176; Fluka) or sodium ionophore II cocktail A (cat. no. 71178; Fluka), and hydrogen ionophore I cocktail B (cat. no. 95293; Fluka) were used for potassium-, calcium-, sodium-, and proton-selective electrodes, respectively. All ISEs were calibrated before use with standard solutions that were prepared by adding desired concentrations of ions into the same solutions employed in experiments (i.e., with either the bath solutions or the pipette solutions, as appropriate). All calibrations are based on incremental changes of ion concentrations in the solutions used in experiments with no attempt to adjust for activities. The slopes of potassium-selective electrodes were 57–58 mV for 10-fold changes of potassium concentration from 0.1 mM to 1 M. The slopes of sodium-selective electrodes using sodium ionophore I were 33–35 mV per decade in the range of our measurements from 0.5 to 0.7 mM sodium in the absence of calcium (120 mM NMG, 5 mM KCl, 1 mM EGTA). The slopes of sodium-selective electrodes using sodium ionophore II were 37–39 mV per decade in the range of our measurements from 2 to 3 mM sodium in the presence of calcium (1 mM with 120 mM NMG). The average slope of proton-selective electrodes was 58 mV from pH 5.5 to 10. The slopes of calcium-selective electrodes were 27–28 mV over the entire pCa range from 2 to 7. The calcium standard solutions for pCa 7 and pCa 6 were prepared with 1 mM EGTA (Sigma-Aldrich) and $CaCl_2$ (Orion, 922006) using published EGTA buffer constants (Collins et al., 1992). To prepare solutions containing >3 μM free calcium, the desired amount of $CaCl_2$ solution was added to solutions without any calcium buffer, and free calcium concentrations were calculated from our estimate of background free calcium in the same solution. The response slopes of the borosilicate and the quartz electrodes were very similar when silanization was successful.

Recording Chamber and the Patch Pipette Oscillation

To measure ion gradients from the cytoplasmic face of excised patches, a recording chamber was employed that allows rapid solution changes with temperature control of the superfusion solution (see Fig. 1 A). The ISEs were mounted with sticky wax in a 1.3-mm wide slit at an ∼15° angle to the horizontal axis (e). The electrode tip protruded into the recording area (d) between the openings of two polyethylene solution inflow lines. A fine chlorided silver wire was then inserted into the back-filled electrolyte solution and connected to the probe of a high input resistance (10^{15} Ohms) electrometer (FD223; WPI). The polyethylene delivery solution lines (a; 0.25 mm i.d.) and the recording area itself (2.5-mm wide, 4-mm deep, 6-mm long, volume 60 μl) were water-jacketed (g), and the solution inflow lines entered the recording area from either side. Temperature of the superfusion solution within the recording area was 34–35°C during all recordings presented.

The recording area of the chamber communicated with a much larger chamber area into which isolated cardiac myocytes were initially dispersed (c; 20-mm wide, 4-mm deep, 15-mm long, 1.2 ml volume) and in which seals were formed and patches were excised. The large chamber communicated with the recording area via an intermediate chamber (6-mm wide, 4-mm deep, 20-mm long, volume 0.48 ml). After excising a patch, the chamber was manipulated via the microscope stage so that the patch pipette tip was brought to a position just in front of the ISE. Then, the bathing solution was drawn out of the large chamber area (f), leaving a thin layer of solution on the bottom and edges to provide electrical connection to the patch clamp and the electrometer, usually via a 3 M KCl agar bridge (h). When using potassium-selective electrodes a 3 M NaCl agar bridge was employed to avoid any possibility of potassium contamination. Solution level in the narrow recording chamber area remained high due to solution adhesion to the narrow walls. Solution changes were made by applying pressure to the appropriate solution input line via a syringe reservoir (unpublished data). During application of a new solution, the solution dispersed smoothly into the intermediate chamber area and was subsequently removed via a suction pipette placed in the prechamber area. As illustrated in Fig. 1 B, the patch pipette tip was positioned just in front the of ISE tip, and it was then moved laterally between two positions at a variable distance in the z-axis. In this way, the set-up requires only one micromanipulation system. The standard movement (a to b) was 50 μm, applied manually through a Huxley-type micromanipulator on which the patch pipette was mounted. The movement was typically complete in 0.5 s. Mechanical drift of the manipulator is entirely negligible for the time scales of measurements described in this article, and our best-estimate is that the position of the patch pipette with respect to the ISE tip is accurate to within 2 μm. The specific reasons for drift of ISE signals in our recordings are unknown, except that they are inherent to the ISEs as prepared by us.

Extracellular (Intrapipette) ISEs

Fig. 2 shows schematically the placement of the ISE (d) in the patch pipette (f). The pipette holder (a) was cut and glued to form a 135° angle in the connector path to the patch pipette (c). In this way, the pipette formed a 45° angle to the bath chamber bottom when the holder was mounted horizontally, as indicated. A small hole was drilled through the glued joint to allow the relatively straight passage of a polyethylene tube (b) through the holder and into the patch pipette. As mentioned above, this tube served as a guide to allow easy retrograde placement of the ISE into the pipette holder, and it served as a shield during the replacement of patch pipettes. The ISE could then be manipulated by hand (i) to a short distance from the patch pipette tip, and with experience the tip could be placed at accurate distances from the tip as desired. The upper end of the guiding polyethylene tube fitted snugly through an ∼1-cm long piece of glass tubing (c) that was glued into the electrode holder, thereby keeping the quartz electrode nearly straight when manipulated. After the quartz electrode was inserted, negative pressure could be applied to the patch pipette through the holder (h) with minimal solution and air leak through the connections. As necessary, soft wax was used to seal the polyethylene tube and capillary electrode (b).

After retrograde fitting of the capillary electrode through the polyethylene tube, a fine chlorided silver wire was inserted into the quartz electrode for connection to the probe of the electrometer, and the electrode was allowed to equilibrate for 10–15 min with the experimental solution. The slope of the electrode was

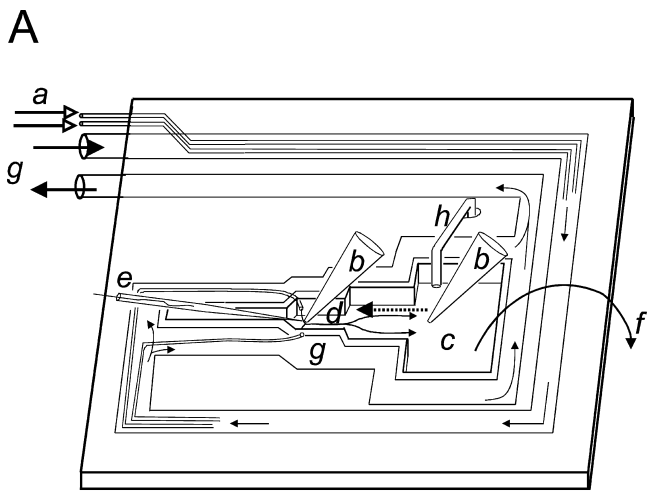

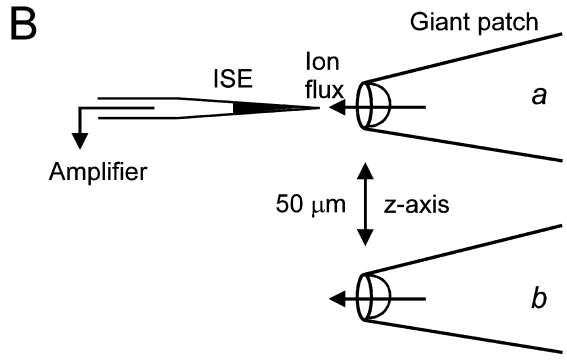

FIGURE 1. Schematic representations of ion flux measurements from the cytoplasmic side. (A) Diagram of temperature-controlled recording chamber used in experiments. Solution is pressed from syringes (not depicted) through two polyethylene tubes (a, see open arrow bars; 0.25 mm i.d./0.6 mm o.d.) into the recording area (d). Seal formation and excision of the giant patch membrane (b) are achieved within a larger chamber where the cells are placed initially (c). The patch pipette tip is then moved into the temperature-controlled recording chamber (d, see dotted arrow bar) and brought into the front of the ion-selective microelectrode (e), which is attached on the recording chamber by sticky wax. Subsequently, bathing solution in the larger chamber is drawn out by suction through a syringe (f; not depicted). The recording chamber is surrounded by a water jacket with the flow path indicated by arrows (g). The polyethylene tubes for adding solution to the recording chamber are pointed at the patch from opposite sides, and the injected solution flows out into the larger chamber (c) from where it is removed by suction (f). A reference agar bridge electrode (h) is placed into the larger chamber at its edge. (B) Schematic representation of the patch pipette movement. The patch pipette tip orifice (a) is positioned ~4 μm away from the center of ISE and repeatedly moved back and forth laterally in the "z-axis" (b). The standard oscillation distance is 50 μm which effectively allows measurement of the entire concentration gradient as recorded by the ISE.

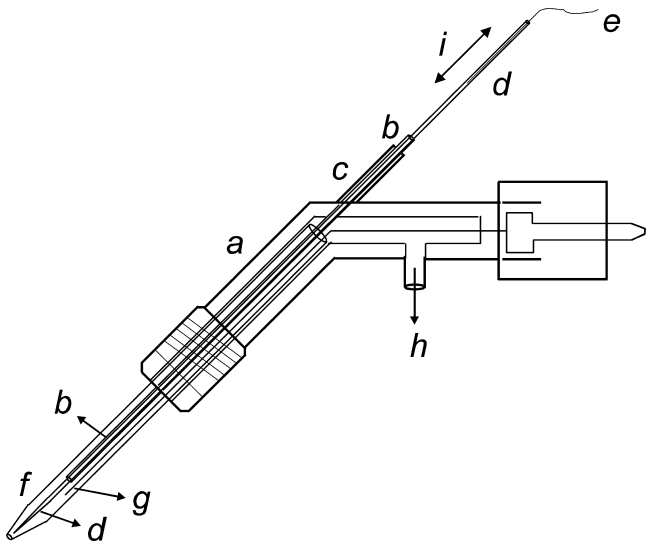

FIGURE 2. The intrapipette (extracellular) ion-selective microelectrode. The plexiglass body of the pipette holder is cut and glued so as to form a shallow angle with respect to the chamber bottom. A hole allows a polyethylene tube (b, 1 mm o.d., 0.35 mm i.d.) to be inserted snugly into the holder, and the upper end of the polyethylene tube tights tightly into 1-cm glass pipette (c) glued into the hole from the top. The ion-selective microelectrode (d, 350 mm o.d., 200 mm i.d.), fabricated from quartz capillary tubing, is inserted from the bottom through the polyethylene tube, and a thin silver wire (e) is inserted into the ISE from the top and connected to the electrometer. Then, giant patch pipette (f) is carefully inserted over the polyethylene tube and into the holder with the active silver wire of the patch clamp as guide (g). During seal formation, negative pressure is applied through a suction line (h), and after seal formation the microelectrode is moved by hand any desired distance from the patch membrane (i). Positioning of the ISE causes large electrical artifacts (not depicted), but almost never destabilizes the patch seal.

then measured with the solution standards. When changing patch pipettes, the quartz electrode was drawn into the polyethylene tubing, and then a prefilled patch pipette was carefully fitted over the polyethylene tube into the electrode holder without touching the tip of the quartz electrode. During this procedure, the chlorided silver wire of the patch clamp electrode (g) served as a convenient physical guide, as it extended just beyond the polyethylene tube. The final distance between the pipette tip orifice and the electrode tip was calibrated by two methods; first, via a reticule in the microscope eye piece with compensation for the pipette angle with respect to the chamber, and second, via the calibrated length of the ionophore column as described above.

Giant patches were formed by the general methods described previously (Collins et al., 1992). To prevent any contamination of pipette solutions by bathing solutions during seal formation, the myocytes were placed into the pipette solutions for seal formation. Before filling, the empty patch pipettes were briefly dipped into a highly viscous mixture of Parafilm and light and heavy mineral oils (Collins et al., 1992). With this glue and with relatively straight-tip patch pipettes, seal formation was fast with gentle suction, and the membrane could usually be accurately visualized in the pipette tip. Usually, the membrane relaxed into a position a few μm (3–6 μm) from the pipette tip orifice, and knowledge of this position allowed accurate calibration of the distance between the membrane and the ISE. After patch excision, the pipette was lifted and the ISE was carefully manipulated by hand to the desired distance from the membrane. Thereafter, the pipette was moved into a recording chamber as described previously (Collins et al., 1992). After measuring ion fluxes at

35–36°C, the patch pipette was removed carefully and the dimensions of the patch pipette were carefully measured for subsequent simulation of diffusion and calculation of the ion fluxes. Finally, the slope of the ISE was measured again and compared with the slope measured before the experiment. Changes of the slope were identified in ~5% of the electrodes, and the data from those experiments were discarded.

Patch Pipettes and Controls for "Tip Potential" and Liquid Junction Potentials

The patch pipettes used to form giant patches were prepared to have nearly conical shapes with relatively small tip angles (i.e., with very light fire polishing after cutting). As described subsequently, nearly conical pipette tips allow ion concentration changes to be simulated easily, and relatively narrow pipette tips promote ion accumulation. A disadvantage of narrow pipettes is that the tip resistances are relatively high (0.2–0.4 MΩ), as compared with highly polished (melted) giant pipette tips (<0.2 MΩ). Accordingly, the development of a tip potential during the activation of large membrane currents is a possible concern. Both the tip potential and liquid junction potentials can be expected to be monitored by the intrapipette ISE. To directly test the possible influence of these artifacts, two types of controls were performed. First, a quartz capillary electrode without resin, and filled with the patch pipette solution, was used to measure the potential in the pipette tip. Upon activating a 3 nA potassium current with valinomycin, as in Fig. 11, the potential change measured by the quartz capillary electrode was just 0.8 mV. More than one-half of the potential measured depended on the presence of a large current (i.e., valinomycin). The tip potentials developed immediately upon changing solutions (i.e., in <1 s) and decayed similarly quickly upon deactivating the current, which contrasts strongly with the time-dependent ion accumulation signals described. Second, we checked the liquid junction potentials induced by solution changes, using small diameter patch pipettes in current-clamp mode. Liquid junction potentials were minimized, whenever possible, by choosing ion substitutions so that the conductivities of the different solutions were equal. The measurements of potassium fluxes in the presence of valinomycin (Fig. 11) are the only case in which liquid junction potentials are quite large (~2 mV) due to the exchange of potassium for NMG. However, the ISE responses are much larger in those measurements. Based both on the measurements and calculations, we are confident that potentials related to access resistance and liquid interfaces remain very small with respect to the ISE responses described in this article.

Solutions

The pipette solution for the potassium influxes mediated by inward potassium channel currents contained (in mM): 140 KCl, 3 $MgCl_2$, 0.15 ouabain, 20 HEPES (pH 7.0 with MES). Cytoplasmic superfusion solution for the potassium channel current contained (in mM): 140 choline chloride, 0.18 KCl, 20 HEPES (pH 7.0 with MES). For measuring potassium influxes mediated by forward mode of Na/K pump transport, the pipette solution contained (in mM): 5 KCl, 100 NMG, 4 EGTA, 40 TEA-OH, 15 CsOH, 4 $MgCl_2$, and 20 HEPES (pH 7.0 with MES). The cytoplasmic superperfusion solution for the pump current contained (in mM): 10 NaCl, 0.1 KCl, 100 NMG, 5 EGTA, 1 $MgCl_2$, and 20 HEPES (pH 7.0 with MES). The pump current was activated upon addition of 1 mM MgATP and turned off upon removal of MgATP. The pipette solution for the valinomycin-induced outward potassium current contained (in mM): 0.5 KCl, 120 NMG, 0.15 ouabain, 1 $MgCl_2$, and 10 HEPES (pH 7.0 with HCl). The bath solution for the valinomycin-induced potassium current contained (in mM): 120 KCl, 2 EGTA, 1 EDTA, 1.5 $MgCl_2$, and 10 HEPES (pH 7.0 with NMG). To turn off the potassium current, the cytoplasmic solution was replace by the pipette solution. The pipette solution for the calcium influx mode of Na/Ca exchange current contained (in mM): 3 $CaCl_2$, 60 NaCl, 20 NMG, 25 TEA-OH, 0.5 $MgCl_2$, 0.15 ouabain, and 20 HEPES (pH 7.0 with HCl). The superfusion solution for Na/Ca exchange current contained (in mM): 60 or 100 NaCl, 20 CsCl, 40 TEA-OH, 1 $MgCl_2$, and 20 HEPES (pH 7.0 with MES). Then, desired amounts of calcium were added into the superfusion solution to prepare various background cytoplasmic calcium concentration (4.4–32 μM). To turn off the exchange current, sodium in the bath solution was replaced by the same amount of CsCl. The pipette solution for the measurement of sodium fluxes mediated by forward mode of Na/K pump, with the sodium ISE (sodium ionophore I) in the patch pipette, contained (in mM): 120 NMG, 5 KCl, 0.5 NaCl, 1 EGTA, 20 HEPES (pH 7.0 with HCl). The pipette and bath solution for the gramicidin-mediated sodium current contained (in mM): 120 NMG, 1 $CaCl_2$, 2 NaCl, 10 HEPES (pH 7.0 with HCl). To activate sodium current through gramicidin channels, 15 mM Na-gluconate was added to the cytoplasmic solution. The cytoplasmic superperfusion solution for the pump current contained (in mM): 10 NaCl, 20 CsCl, 50 NMG, 40 TEA-OH, 1.5 $MgCl_2$, 10 EGTA, 1 EDTA, 20 HEPES (pH 7.0 with HCl). The pipette solution to support the proton-influx mode of Na/H exchange contained (in mM): 150 Choline-Cl (or 150 Cs-aspartate), 3 $MgCl_2$, 0.5 ouabain, 2 $CsCl_2$, and 10 MES (pH 6.2 with CsOH). The superfusion solution to support the proton influx mode of the transporters contained (in mM): 150 NaCl, 1 $MgCl_2$, and 0.05 TRIZMA-base (pH 7.4 with NaOH). When it was necessary, NaCl was replaced by 150 mM choline-Cl at the same pH. The pipette solution that favors the proton efflux mode of Na/H exchange contained (in mM): 150 NaCl, 0.1 5 ouabain, 2 CsCl, 1 $MgCl_2$, 10 TEA-Cl, 0.1 HEPES (pH 7.2 with NaOH). The superfusion solution for the proton efflux mode contained (in mM): 120 CsCl (or 120 NaCl) 20 TEA-Cl, 3 EGTA, 1.5 $MgCl_2$, 1 EDTA, 10 CsCl, and 10 MES. The pH of the bath solution was adjusted to either 6.0 or 7.2 with NMG. The pH levels of all solutions with low pH buffer concentrations were adjusted to the desired values on a daily basis and adjusted as necessary using HCl or NaOH.

Physical Principles, Diffusion Models, and Simulations

Ion fluxes across an excised membrane patch take place in effectively unlimited volumes. As described subsequently in simulations, activation of a constant ion flux across the patch generates ion gradients next to the membrane that approach a steady-state within a few seconds to minutes, outside and inside the pipette, respectively. Thereafter, concentration changes are negligible for many hours. To predict the magnitudes and geometry of the gradients, the extracellular (pipette) side of the membrane can be approximated as a cone or sphere sector, for which analytical solutions can be readily derived. Accordingly, it is important that pipettes are pulled and cut carefully so as to maintain nearly straight walls. The geometry of the cytoplasmic (bath) side of the membrane cannot be approximated by any simple geometry. Therefore, finite difference simulations are required to accurately predict the ion concentration gradients in front of the pipette tip.

Ion Concentration Changes in the Pipette Tip

For the purposes of this article, it is very useful to quantify ion fluxes across the membrane patch as equivalent monovalent cation currents *(I)*. The ion flux in moles per second is then I/F, where F is the Faraday constant. In the steady-state, the concentration gradient (dC/dx) at a distance, x_p, from the pipette orifice

is proportional to the ion flux *(I/F)* and inversely proportional to the diffusion coefficient *(D)* and the area *(A)* of the corresponding sphere sector, $\pi \cdot r_x^2 \cdot 2 \cdot (1 - cos\theta_{1/2})/tan^2\theta_{1/2}$, where r_x is the pipette cross-sectional radius at the distance, x_p, from the pipette orifice, measured parallel to the center axis of the pipette, and $\theta_{1/2}$ is the angle formed between the patch pipette wall and the axis of the pipette (see Fig. 3).

$$dC/dx = I/(F \cdot D \cdot A). \quad (1)$$

Most results described in this article were obtained using pipettes with $\theta_{1/2} < 5°$. With these narrow pipettes, the cross-sectional area of the pipette, $\pi \cdot r_x^2$, can be substituted for the area of the sphere sector in Eq. 1 with a maximal error of only 0.2%. Relevant to simulations described in Fig. 7, the error is 1.1% at 12°. Here, as in subsequent equations, concentration units are moles/ml when the current equivalents are in amperes, distances are in cm, and D is in cm^2/s. Multiplication of moles/ml by 10^9 converts concentration units to micromoles/liter (μM).

The steady-state ion accumulation (C_x) in the pipette at a distance, x_p, from the pipette orifice having the radius, r_t, is obtained by integrating Eq. 1 from x_p to infinity. Eqs. 2 and 3 give the results using the sphere sector and the cross-sectional areas, respectively. The tangent function in Eq. 2 should be replaced by the sine function when the radial pipette length is measured (i.e., directly along the side of the pipette). Differences between these results are, however, all insignificant for results considered in this article with $\theta_{1/2} < 5°$.

$$\Delta C_x = I/[F \cdot D \cdot \pi \cdot 2 \cdot (1 - \cos\theta_{1/2}) \cdot (r_t/\tan\theta_{1/2} + x_p)]. \quad (2)$$

$$\Delta C_x = I/[F \cdot D \cdot \pi \cdot \tan\theta_{1/2} \cdot (r_t + x_p \cdot \tan\theta_{1/2})]. \quad (3)$$

In some experiments to be described, ion concentrations in the patch pipette are measured at multiple distances from the pipette orifice. Therefore, an equation is useful to predict the concentration difference from the distance between the two points of measurement, x, and the corresponding pipette radii, r_1 and r_2. This equation can be derived from Eqs. 2 or 3:

$$\Delta C = I \cdot \Delta x/(F \cdot D \cdot \pi \cdot r_1 \cdot r_2). \quad (4)$$

To calculate ion accumulation over time *(t)*, after activating an ion flux, an analytical solution for the sphere sector model was derived. The concentration at a distance, x_p, from the tip orifice, $C_x(t)$, is calculated with assumption of a homogeneous background concentration in the pipette at time zero, C(0).

$$\alpha = 0.5 \cdot x_p/sqrt(D \cdot t). \quad (5)$$

$$\beta = \alpha + sqrt(D \cdot t \cdot \sin\theta_{1/2}/r_t). \quad (6)$$

$$\gamma = (x_p + D \cdot t \cdot \sin\theta_{1/2}/r_t) \cdot \sin\theta_{1/2}/r_t. \quad (7)$$

$$C_x(t) = \Delta C_x \cdot [erfcc(\alpha) - erfcc(\beta) \cdot \exp(\gamma)] + C(0). \quad (8)$$

Here, ΔC_x is the result of Eq. 2; α, β, and γ are temporary variables; and erfcc is the complementary error function. The results from Eq. 8 were practically identical to results from one-dimensional discrete simulations described subsequently when $\theta_{1/2}$ was <12°.

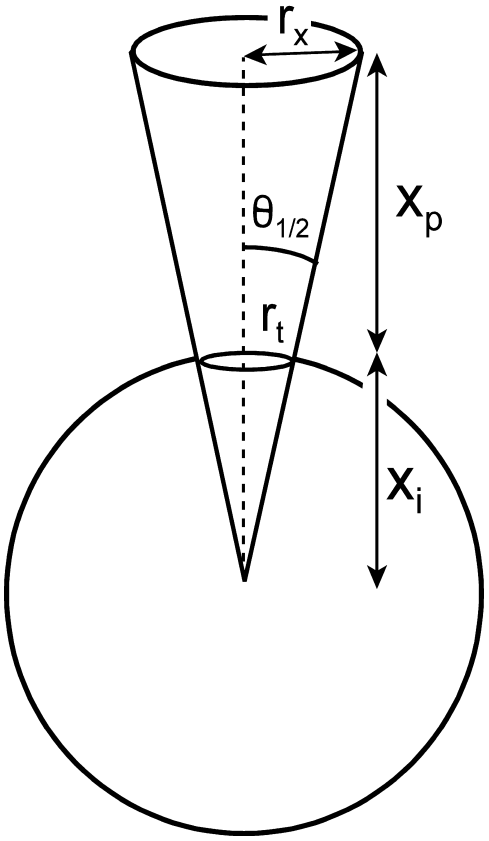

FIGURE 3. Diffusion model for patch pipette with a conical shape. The pipette defines a sphere sector with $\theta_{1/2}$ being the angle formed by the pipette wall with respect to the center axis. The membrane is assumed to be located in the orifice of the pipette tip with the radius, r_t, at a distance, x_i, from the center of imaginary sphere ($x_i = r_t/\sin\theta_{1/2}$). The pipette radius, r_x, at any distance from the pipette orifice, x_p, is $(x_i + x_p) \cdot \sin\theta_{1/2}$. See text for further explanations.

For some purposes, the response of the ISE was simulated in millivolts (*Ve*). To do so, the electrode response for a 10-fold change of concentration, (V_{10}), was extrapolated from its response for a small concentration change, usually 20% above the background concentration, *C(0)*.

$$V_e = V_{10} \cdot \log[C_x(t)/C(0)]. \quad (9)$$

Discrete (finite difference) simulations are required to predict ion concentration changes for more complex experimental protocols (e.g., multiple changes of transport activity), for more complex pipette geometries (i.e., nonconical shapes), and to make predictions for the cytoplasmic side. For the pipette side, simulations were performed in both one and two dimensions. For pipette tips with half-angles <15°, the results of two-dimensional simulation schemes were not different from those for one-dimensional schemes in any respect significant for this article (not depicted). The maximum differences between the one- and two-dimensional simulations were <2% when $\theta_{1/2}$ was <12°.

For one-dimensional simulations, the pipette was divided into imaginary compartments bounded by planes perpendicular to the central axis of the pipette. Initially, simulations were per-

formed assuming a conical tip dimension. However, small deviations from the conical shape, in particular flaring-out of the pipette tip distances >0.3 mm from the orifice, were found to significantly affect the simulations. Specifically, the cone model consistently overestimated ion concentration changes in the tip, whereby $\theta_{1/2}$ was determined by a least squares method, in comparison to a more accurate reconstruction of the pipette dimensions. Several equations were tested to reconstruct the inside pipette dimensions, using the least squares method to obtain optimized parameters. Especially for pipettes tips that had been melted to decrease access resistance, relatively complex functions were required. A sum of three power functions allowed precise reconstruction of all pipette shapes. Usually, one linear component was included in the fitting equation, as follows:

$$r_x = r_t + k_1 \cdot x_p + k_2 \cdot x_p^{k3} + k_4 \cdot x_p^{k5}. \quad (10)$$

The best fit of Eq. 10 was then used to recreate the pipette dimensions in the finite difference simulation. Also, this equation was used to reconstruct the pipette tip dimensions and then to calculate the steady-state ion concentration profile in the pipette by integrating Eq. 1.

For discrete simulations, the concentration change (C) per time step (t) is calculated from the radii, r[1] to r[n], the corresponding areas, a[1] to a[n], and the compartment volumes, v[1] to v[n]. With i as the compartment index, the radii, r[1] to r[n], are equal to $r_t + \Delta x \cdot i \cdot \sin\theta$ for a conical pipette, where Δx is the discretization length. The area, a[i], is then $\pi \cdot r[i]^2$, the volume, v[i], is $\Delta x \cdot 0.5 \cdot (a[i+1] + a[i])$ and the concentration change per time step is,

$$\Delta C[i]/\Delta t = \{(C[i-1] - C[i]) \cdot a[i-1] + (C[i+1] - C[i]) \cdot a[i]\} \cdot D/(\Delta x \cdot v[i]). \quad (11)$$

The membrane is assumed to form the boundary of the compartment with the smallest radius (i = 1), and the corresponding differential equation (i.e., C[1]/t) is modified by addition of the ionic flux, I/F, and by absence of a flux component to a smaller neighboring compartment. At the opposite boundary (i = n), the differential equation for C[n] is modified by omission of a flux component to a larger neighboring compartment (i.e., equivalent to an air–water interface). The distances, over which the simulations were performed, are selected long enough, usually >1 mm, so that diffusion to the outer boundary remains negligible. Effects of the simulation distance and results for long-time simulations are described in RESULTS. Both a semiimplicit method (Hilgemann and Lu, 1999) and a Runge-Kutta midpoint method (Press et al., 1986) were used for integration with no significant differences.

To model diffusion on the cytoplasmic side of the pipette, a two-dimensional diffusion model is used in which the discrete unit is a ring of equal thickness and width, x, that communicates with four adjacent rings. Accordingly,

$$\Delta C[i,j]/\Delta t = \{a'[j] \cdot (c[i+1,j] + c[i-1,j] - 2 \cdot c[i,j]) + a''[j+1] \cdot (c[i,j+1] - c[i,j]) + a''[j] \cdot (c[i,j-1] - c[i,j])\} \cdot D/(\Delta x \cdot v[i,j]), \quad (12)$$

where i is the longitudinal compartment index (i.e., along the axis of the pipette), j is the index in the radial direction, a′[j] is the area of the lateral face of the ring at radial index, j, and a″[j] is the area of the inner face of the ring at the radial index, j. At all compartments facing the patch pipette, as well as facing the assumed membrane, one of the four diffusion components is removed from the respective equation, as appropriate. The transmembrane ion flux (I/F) is partitioned between all of the compartments facing the membrane in proportion to their respective areas, a′[j]. The steady-state concentration profiles, when desired, were calculated by an iterative Newton method.

RESULTS

Simulations of Ion Gradients

Fig. 4 shows the steady-state ion gradients predicted outside of a straight patch pipette tip with a radius of 7.5 μm. The results presented are for a 40 pA inward (i.e., flowing from the pipette) potassium current, assuming a potassium diffusion coefficient of 2.03×10^{-5} cm^2/s (37°C), projected from a value of 1.96×10^{-5} cm^2/s at 25°C (Robinson and Stokes, 1965). The membrane in this simulation is assumed to be a flat disk surface recessed 5 μm into the pipette tip. The position of the membrane within the pipette tip has no influence on the ion concentrations outside the recessed area. Changes of the current magnitude or the diffusion coefficient affect only the steady-state concentrations, not the normalized concentration profiles.

Fig. 4 A shows the predicted concentration profiles perpendicular to the axis of the pipette. Gradients are shown for three planes: 1 μm from the tip of the pipette, 3 μm from the tip, and 10 μm from the tip. The peak concentration at the 1-μm plane is 6.7 μM, and the ion accumulation falls off by 80% over a distance of <20 μm from the center axis. Fig. 4 B shows the predicted accumulation profiles along center axis of the pipette (0 μm) and along an axis just outside the pipette (8 μm). For orientation to the graph, the plane of the membrane and the plane of the pipette tip are indicated by vertical dotted lines. Following the gradient from the membrane, along the center axis, ion accumulation decreases in a linear fashion within the pipette tip, as expected for an ion flux through a cylinder. But once outside the pipette tip, the gradient falls off less sharply in a nearly exponential fashion along the pipette axis, roughly with a space constant equivalent to the pipette radius, 7.5 μm. Following the gradient along the outside edge of the pipette, the ion accumulation falls off somewhat more steeply toward the pipette shank than in the direction away from the pipette tip.

Does the ion gradient in front of the pipette tip allow accurate quantification of the ion flux across the patch membrane? Fig. 5 shows the ion concentration along the central axis of the pipette tip at the indicated distances from the pipette orifice. The gradient is reasonably well described by a decaying exponential function. As already noted, the gradient outside of the pipette is not affected by the position of the membrane in the pipette, and the influence of the pipette tip angle is also negligible. Thus, the gradient depends only on the ion flux magnitude, the diffusion coefficient, and the pi-

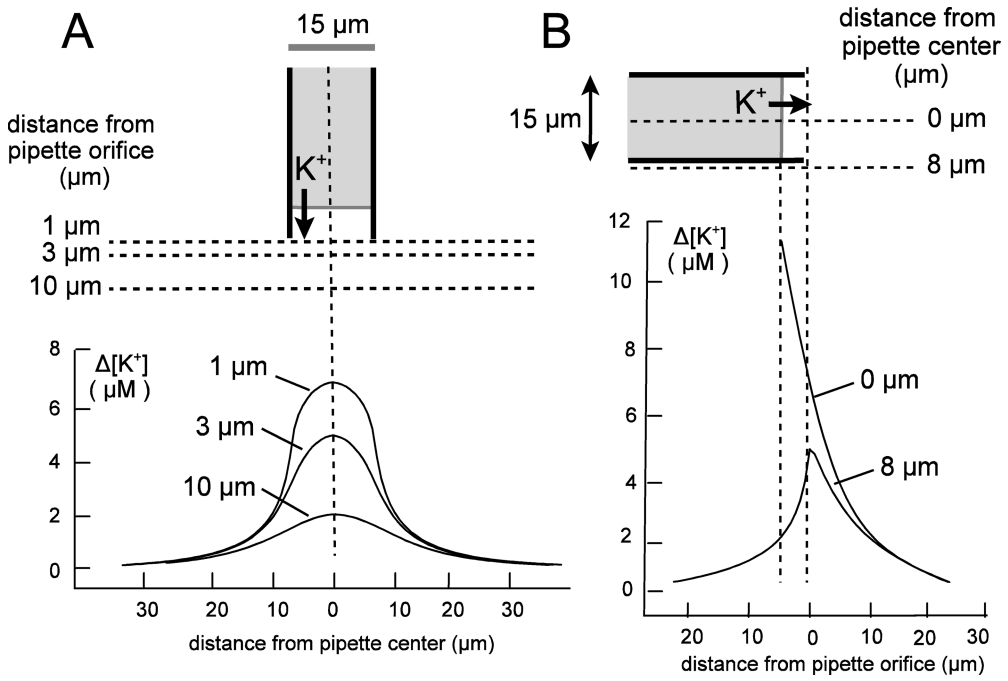

FIGURE 4. Predicted ion gradients on the cytoplasmic side of a patch pipette. The patch pipette is assumed to be cylindrical, and the membrane is recessed from the pipette orifice by 5 µm. The pipette diameter is 15 µm, and the gradients are calculated for a 40 pA inward potassium current. The potassium diffusion coefficient is 2.03×10^{-5} cm^2/s. (A) Ion gradients expected in three planes perpendicular to the center axis of the pipette, namely 1, 3, and 10 µm from the pipette tip. (B) Ion gradients expected in a plane that transects the axis of the pipette (0 µm) and in a parallel plane just next to the pipette wall (8 µm). See text for further explanations.

pette diameter. To describe the gradient in front of the pipette empirically, an exponential function (dotted line in Fig. 5) was fitted to the simulated gradient along the pipette axis.

$$\Delta C = [I/(F \cdot D \cdot \pi \cdot r_t \cdot k_1)] \cdot \exp(-k_2 \cdot x_0/r_t). \quad (13)$$

Here, x_o is the distance from the pipette orifice and k_1 and k_2 are constants. Using a least-squares method to fit the equation to simulated datasets, the best fits for k_1 and k_2, respectively, were 1.26 and 1.10.

These simulations support the feasibility of making accurate flux estimates from measurements of concentration gradients. The normalized concentration profiles in steady-state are determined by the geometry of the diffusion space, not by the diffusion coefficients. The magnitudes of ion accumulation can be accurately predicted even when analytical solutions of diffusion equations are not possible. For the cytoplasmic side of the patch, ion accumulation will be somewhat greater than expected for the surface of a hemisphere with the radius of the pipette tip ($\Delta C = I/[F \cdot D \cdot \pi \cdot 2\, r_t] = 4.2$ µM for the parameters of Fig. 4). In experiments, the ISE can be positioned reliably at 3–5 µm from the pipette orifice. For the purposes of this article, we attempted to standardize the pipette tip radius at 7–8 µm and to position the pipette tip orifice accordingly at 3–4 µm from the ISE. Therewith, for pipette tips with 7.5 µm radii, Eq. 13 predicts an accumulation of 0.10 µM/pA for a current carried by potassium (i.e., with a diffusion constant of 2.0×10^{-5} cm^2/s), and 0.25 µM/pA for a monovalent cation with a diffusion constant of 0.8×10^{-5} cm^2/s (i.e., equivalent to calcium).

Fig. 6 presents the ion gradients predicted to occur within the pipette tip when a 40 pA outward potassium current (i.e., into the pipette) is activated. The pipette tip radius is assumed to be 7.5 µm, the half-angle ($\theta_{1/2}$) of the tip is assumed to be 12° (see Fig. 6 A), and the diffusion coefficient for potassium (at 37°) is assumed to be 2.03×10^{-5} cm^2/s. Results are shown for both the analytical solution (Eqs. 5–8) in Fig. 6 B and for discrete simulation in Fig. 6 C. The 12° angle is larger than for any of the pipettes employed in experiments, and simulation results for current activation are very similar. With this relatively wide pipette tip (i.e., 24°), the potassium concentration increases by 40 µM next to the membrane with a half-time of a few seconds. The time needed to reach 90% of steady-state is 8–20 s at distances of 1–100 µm from the membrane. Using the discrete method to simulate further step changes of the current, Fig. 6 C shows that the pipette potassium concentrations return nearly to baseline over a time course similar to that with which accumulation occurs. When the diffusion coefficient is smaller, or when the pipette tip is more narrow, ion accumulations are larger and they occur and dissipate more slowly. Fig. 6 D shows the predicted steady-state concentrations of potassium for Eq. 2 as curve 1, and the integration of Eq. 4 along the pipette tip as curve 2. With this wide angle, the potassium concentration falls off quite steeply in the pipette, so that the exact positions of the membrane and of the ISE are important variables in experimental results. For this reason, we chose to use pipettes with smaller angles of descent.

The fact that a steady-state ion gradient develops during continued ion flux into the pipette can be counter-

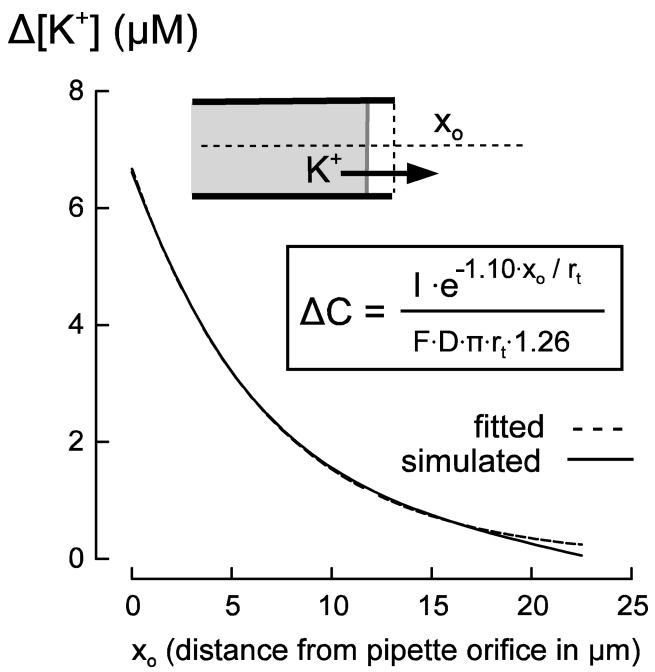

FIGURE 5. Predicted ion gradient in front of a pipette with a 7.5 μm radius in the presence of a 40 pA potassium current. This solid line is the simulated data from Fig. 4. The dotted line is calculated from the expression given in the figure, which recreates well simulated results for different pipette radii, diffusion coefficients, and monovalent cation current magnitudes.

intuitive. Therefore, we describe without figures the results of simulations in which the entire contents of a pipette tip are accounted for. Briefly, the pipette tip dimensions just described were simulated over 2.4 mm as a cone shape, at which point the pipette diameter is 1 mm, and then the pipette was simulated further as a cylinder of 1 mm diameter over an additional distance of 8 mm. With this geometry, the potassium concentration in the tip increases from 38 μM at 2 min (see Fig. 6 B) to 44 μM at 24 h. The concentration increases above the value predicted for the steady-state simulation (40 μM in Fig. 6 D) because at 24 h potassium ions have begun to reach the boundary of the solution in the pipette (i.e., the air-water interface), and they have accumulated to a concentration increment of 4 μM at the boundary. Over the next days and months of simulated time, the ion concentrations increase equally throughout the pipette, while the concentration differences with respect to the boundary, described in Fig. 6 D, are maintained precisely. The potassium concentration in the tip reaches 85 μM on the 112th day, at which time the concentration at the opposite boundary to air has reached 44 μM.

Fig. 7 describes the effect of the pipette angle on the kinetics (Fig. 7 A) and steady-state amplitude (Fig. 7 B) of ion accumulation. The results in Fig. 7 A were generated with Eqs. 5–8; those in Fig. 7 B for steady-state were generated from Eq. 2. The magnitude of ion accumulation is inversely proportional to the half-angle of the pipette over the range of 12° to 3°, and the time to reach steady-state ion accumulation (Fig. 7 A) becomes longer with decreasing angle, as does the time course for its dissipation after stopping the flux (unpublished data). At still smaller half-angles, the simulation results become equivalent to those for ion flux into a cylinder (unpublished data). As illustrated by these results, a smaller angle results in larger accumulations of ions for the same ion flux, and a small angle results in a less steep ion gradient within the pipette. Both of these factors are favorable for the measurements. First, resolution is increased by the larger ion accumulations and, second, the exact position of the ISE in the patch pipette becomes less critical for calibration of fluxes. At angles <2°, however, the long times needed to reach steady-state become prohibitive for routine measurements. Therefore, we used pipettes with half-angles in the range of 3° to 4° for measurements of outward membrane ion flux described in this article.

Cytoplasmic Measurements: Potassium Fluxes Mediated by Potassium Channels and Na/K Pump

We first tested whether potassium fluxes mediated by potassium channels and the Na/K pump could be detected and quantified from the cytoplasmic side using a potassium-selective electrode. The major prediction of this test is that approximately two potassium ions will be transported for each charge moved by the sodium pump due to its 3Na/2K stoichiometry, while only one potassium ion moves across the membrane per charge moved in a potassium channel. Typical results for using giant patches from mouse myocytes are presented in Fig. 8 using patch pipettes with 15 μm diameters. In these experiments, either choline (Fig. 8 A) or NMG (Fig. 8 B) was used as the major cytoplasmic-side cation, and no other monovalent cation except potassium was present on the extracellular (pipette) side. The ISEs were calibrated in the same solutions used in experiments, using 0.1 mM potassium concentration increments.

When a giant cardiac patch is removed from a freshly isolated cardiac myocyte, a large potassium conductance usually develops quickly and then decays slowly over minutes. This conductance represents with good certainty the activities of both K_{ATP} and the inward rectifier potassium channels. As illustrated in Fig. 8 A, a large inward potassium current is recorded at 0 mV when the patch pipette contains a high potassium concentration (140 mM) and the bath solution has a low potassium concentration (0.18 mM in Fig. 8 A). In this case, 140 mM choline chloride, rather than NMG, was

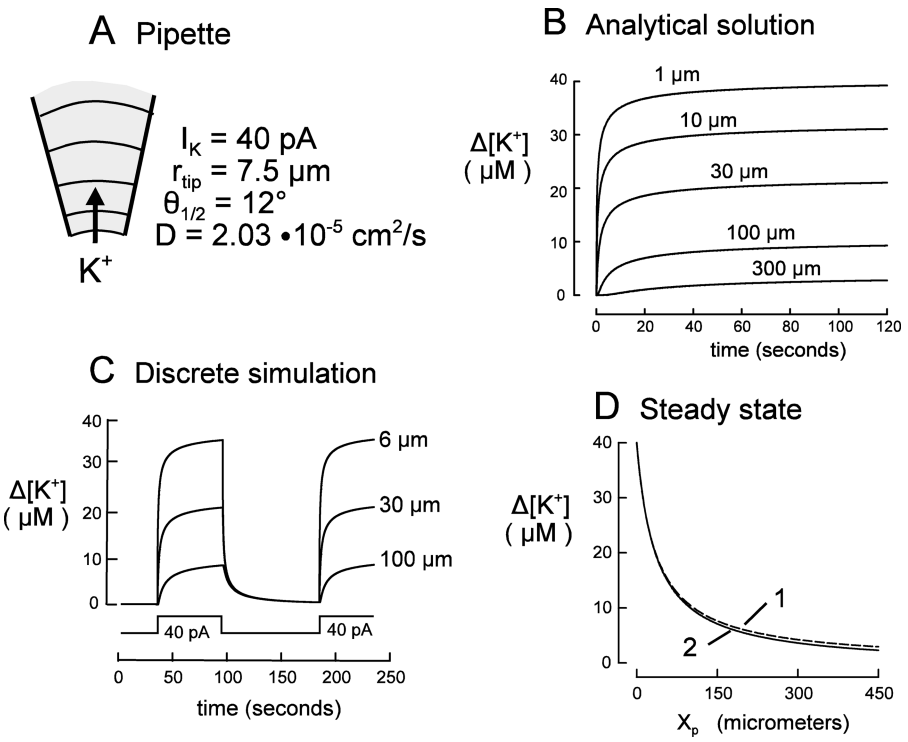

FIGURE 6. Simulated potassium accumulation in a pipette tip during the activation of outward potassium current. (A) Simulation details. A 40 pA outward potassium current is simulated with a pipette tip radius of 7.5 µm and a wall angle of 12° with respect to the pipette axis. (B) Concentration changes over time at given positions along the pipette tip for current activation according to the equations described in the text. (C) Concentration changes predicted by discrete simulation of diffusion in the pipette tip. The potassium current is activated after 30 s, turned off at 90s, and activated again at 180s. Note that the ion concentrations at the different positions equilibrate almost completely within 1 min with the simulated pipette angle and diffusion coefficient. (D) Predicted steady-state solution of the equation system used in B (1) and for integration of the ion gradient along the pipette using the diffusion equation given in the text (2).

used on the cytoplasmic side as the major monovalent cation, because NMG was found to have significant blocking actions on the potassium current. To our knowledge, there is no significant current in the patch besides potassium current in this condition, and the current reverses at 0 mV when 140 mM potassium is added to the cytoplasmic side, as at the end of this record.

As shown above the current record in Fig. 8 A, the patch pipette tip was oscillated between a position 4 µm from a potassium-selective electrode (K-ISE) and a position 50-µm lateral to the electrode. While in the "close" position, the pipette was moved in the x- and y-dimensions to find the position that gave the largest voltage deflection. This position is assumed to be the center of the pipette orifice. Although drift of the ISE is significant, over a minute or longer, voltage deflections of 1.2–1.4 mV are recorded reliably and reproducibly upon repositioning the pipette tip every 10 s. The pipette movements were performed slowly enough, ~1 s per movement, so that no "stirring" effects were evident. From calibrations of the same potassium electrode in the same experimental solution, the average potassium concentration difference for the two pipette positions is determined to be 7.4 µM, which corresponds to 0.099 µM/pA. The pipette diameter is 15 µm, and as noted in connection with Eq. 13, a value of 0.1 µM/pA is predicted for potassium current under these conditions. Clearly, this result is in close agreement with the simulation.

Measurement of potassium flux via the Na/K pump, using a potassium-selective electrode, is described in Fig. 8 B. The Na/K pump is thought to have a 3Na/2K stoichiometry and therefore to transport two potassium ions for each net charge moved during steady-state pump activity (Rakowski et al., 1989; Apell and Karlish, 2001; De Weer et al., 2001). The potassium concentration on the cytoplasmic side is 0.1 mM, with 120 mM NMG and 10 mM sodium as the only other monvalent cations. The pipette tip diameter is again 15 µm, and to allow activation of sodium pump current 5 mM potassium is present in the pipette solution. An 18 pA Na/K pump current is activated by applying 1 mM MgATP on the cytoplasmic side, and the current turns off promptly upon removing cytoplasmic ATP. As expected for a well coupled Na/K pump, the current requires the presence of both cytoplasmic sodium and extracellular potassium (not depicted).

The response of the potassium-selective electrode is shown above the current records. Before application of ATP, displacement of the patch pipette away from and back to a position just in front of the ISE results in no response. During application of 1 mM ATP, 0.8-mV deflections are generated upon moving the patch pipette tip to and from a position directly in front of the patch pipette. And after removal of ATP, the response is again ablated. The 0.8-mV response corresponds to an average potassium concentration increase of 4.2 µM. This corresponds to 0.23 µM/pA, which according to Eq. 13 indicates that 2.3 potassium ions move across the membrane

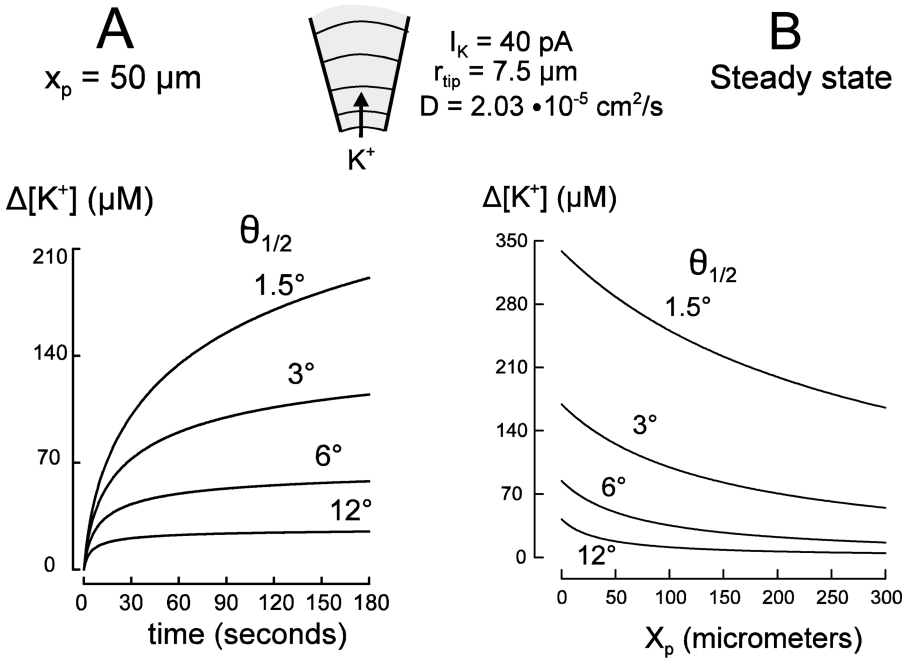

FIGURE 7. Effects of pipette angle on the accumulation of ions during current activation. (A) Predicted results for activation of a 40 pA outward potassium current using pipettes with half-angles of 12, 6, 3, and 1.5 degrees and monitoring [K^+] at a distance (x_p) of 50 µm from the pipette tip. Note that the accumulation becomes larger and reaches a steady-state more slowly as the pipette tip is made more narrow. These results are from the analytical equation system given in the text. (B) Steady-state ion gradients predicted within pipette tips with half-angles of 12, 6, 3, and 1.5 degrees. The results are calculated from Eq. 2, given in the text. Although not obvious in the raw data plots, the gradients fall off more steeply over distance when the pipette tip is wide.

for each charge moved. For a 3Na/2K pump stoichiometry, two potassium ions are expected to move per charge transferred. Thus, these results are in good agreement with the expected Na/K pump stoichiometry.

Cytoplasmic Measurements: Calcium Flux Mediated by Na/Ca Exchange Current

Calcium and proton fluxes are attractive candidates for analysis because ISEs can be used with submicromolar free ion concentrations with the possibility of very large accumulation signals being generated by relatively small ion fluxes. From >10 similar experiments, Figs. 9 and 10 present measurements of calcium flux by reverse Na/Ca exchange. These measurements were selected to illustrate the range of our flux coupling estimates for this system to date. Calcium-ISEs are employed on the cytoplasmic side with no calcium buffer, and 3 mM calcium is present in the pipette. Electrodes and solutions were calibrated with EGTA-buffered standards, and our best estimate of the free calcium concentration of the cytoplasmic solution is 4.4 µM.

Before the signals presented in Figs. 9 and 10 were recorded, the patches were treated with 1.5 mg/ml α-chymotrypsin for 1.5 min to destroy the secondary regulation of the exchanger by cytoplasmic calcium- and sodium-dependent inactivation. As shown beneath the current records in Fig. 9, the outward exchange current was activated by application of 60 mM cytoplasmic sodium in exchange for NMG. The patch was then oscillated in front of the calcium electrode at different cytoplasmic-free calcium concentrations (background $[Ca^{2+}]_i$) to assess the calcium flux. When the pipette tip (15-µm diameter) was moved 50 µm, as described for the previous results, 1.8-mV voltage deflections were recorded in the presence of a 5.5 pA sodium-activated current. We note that this exchange current magnitude is rather small for a giant cardiac patch, and the reason is that the pipettes and sealing procedures employed favored small patches that remain close to the mouth of the pipette tip. We also note that no electrode response was recorded in the presence of 10 mM EGTA at pH 7.0 with 8 mM added calcium (free calcium = 2 µM; not depicted).

The electrode slope was determined to be 28 mV per decade for 10-µM calcium increments above baseline in the experimental solution. Therewith, the concentration changes were determined to be 0.70 µM on average. As shown further in Fig. 9, the measurements were repeated after raising the free cytoplasmic calcium to 32 µM free cytoplasmic calcium, still with 60 mM cytoplasmic sodium, and in this condition the exchange current was decreased slightly to 4.0 pA. 0.2-mV deflections were recorded with the same pipette oscillation, and at the higher background calcium concentration (32 µM) these voltage changes correspond to a 0.53 µM cytoplasmic-free calcium accumulation above baseline. With 14 µM calcium and 100 mM sodium, the exchange current increased to 6.8 pA, and the voltage deflections corresponded to 0.83 µM calcium accumulation above baseline. When the exchange current was turned off by the removal of cytoplasmic sodium at 4.4 µM free calcium, no appreciable calcium gradients could be detected. Even when the patches became rather "leaky" after many minutes of recording, submembrane-free calcium accumulations amounted to

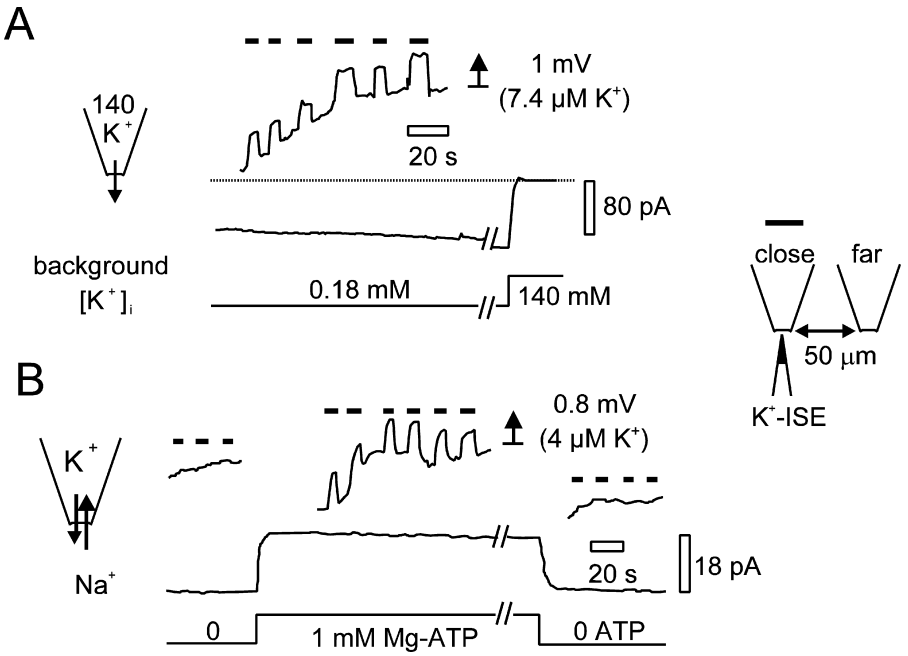

FIGURE 8. Measurement of potassium fluxes mediated by potassium channels and Na/K pumps. (A) Cytoplasmic potassium accumulation induced by potassium channel activity. The patch was excised into 0.18 mM potassium-containing cytoplasmic solution, and the patch pipette contained 140 mM potassium. Inward potassium currents activate spontaneously in this condition, and ion gradients were established as shown above the current record using a potassium-selective microelectrode (K^+-ISE). The patch pipette was moved between a position just in front of the ISE (close) and a position 50 μm away from the ISE in the lateral dimension (far). An average 1-mV voltage deflection was recorded upon repositioning the pipette tip, which corresponds to a 7.4 μM higher potassium concentration in the "close"' position. After these measurements, the current amplitude was checked by substituting 140 mM potassium on the cytoplasmic side for 140 mM chloline, thereby causing a very large deflection of the ISE (not depicted). (B) Cytoplasmic potassium accumulation induced by Na/K pump activity. The pipette potassium concentration was 5 mM, and the cytoplasmic potassium and sodium concentrations were 0.1 and 10 mM, respectively. No ISE electrode response could be recorded before activating the Na/K pump. Pump current was activated by applying 1 mM Mg-ATP on the cytoplasmic side of the membrane in the presence of 10 mM sodium. With 50-μm movements of the pipette, an average voltage deflection of 0.8 mV is recorded. This corresponds to a 4 μM accumulation of potassium at a distance of ~4 μm from the pipette edge. After the current was turned off by the removal of Mg-ATP, voltage changes were again undetectable upon oscillating the pipette in front of the ISE. The solid bars over the voltage traces indicate that the ISE was positioned at the center of the patch pipette during that time. The average magnitudes of voltage deflections are indicated as arrow bars with calculated ion concentration change in parentheses. The direction of the arrows indicates an increase in ion concentration.

no more than 5% of the calcium gradients detected during activation of the exchanger-mediated ion flux.

The ratios of the calcium accumulations to the current magnitudes remain nearly constant under all these different conditions, namely 0.13, 0.13, and 0.12 μM/pA at 4.4, 32, and 14 μM background free calcium, respectively. This suggests therefore that no significant changes of stoichiometry occur with these gradient changes. A 3Na/1Ca exchanger stoichiometry predicts that 1 charge moves across the membrane per calcium ion transported, and according to Eq. 13, with a calcium diffusion coefficient of 0.8×10^{-5} cm^2/s, the calcium accumulation should amount to 0.25 μM/pA. The measured calcium accumulations are only about one-half of the predicted accumulations, and they are therefore consistent with a 4Na/1Ca stoichiometry, as recently suggested by others (Fujioka et al., 2000; Dong et al., 2002).

Fig. 10 presents a second example of recordings of Na/Ca exchange–mediated calcium fluxes. Again, the pipette tip diameter was 15 μm, but in this case a much larger 30 pA Na/Ca exchange current was recorded in the presence of 4.5 μM background calcium. The reason for the larger current is probably that the membrane extended into the pipette substantially further than in the previous figure. The maximum calcium accumulation is estimated to be 6 μM in this experiment. As shown in Fig. 10 A, the patch pipette was moved laterally in front of the calcium electrode in small steps, so as to determine the lateral geometry of the ion gradient. The electrode readings were then converted to calcium concentrations, and the concentrations are plotted in Fig. 10 B as a percent of the maximum accumulation. The shape of the gradient with respect to distance from the pipette axis corresponds reasonably to the predicted profiles in Fig. 4 A for a pipette of the same dimension. The half-maximal accumulation occurs at a distance of 12–15 μm from the center axis, somewhat less than one pipette radius from the edge of the pipette.

In several experiments, we moved the ISE tip into the mouth of the patch electrode to test for the existence of larger calcium accumulations within the pipette tip. Often, small mechanical perturbations occurred during the maneuver, and recordings were not stable. And since we favored seal conditions that leave the membrane patch close to the pipette orifice, the ISE tip often contacted and disrupted the patch. In two recordings, however, we verified that calcium accumulation inside the pipette tip could be at least twice that occurring in front of the pipette tip.

As shown in Fig. 10 C, the peak submembrane calcium gradient was 6 μM when either 4.5 or 7.5 μM background free calcium was present on the cytoplasmic side.

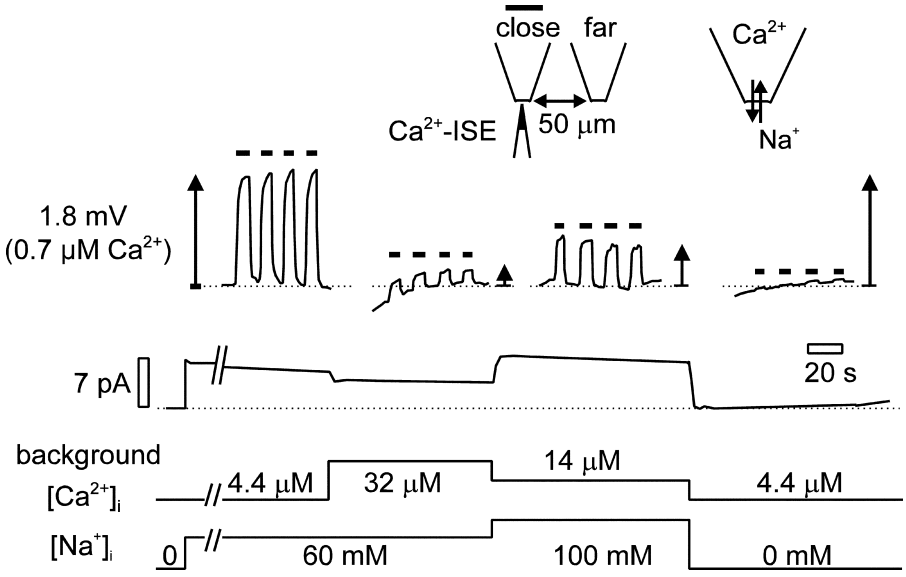

FIGURE 9. Measurement of calcium fluxes mediated by reverse Na/Ca exchange at three cytoplasmic calcium concentrations (background $[Ca^{2+}]_i$) with 3 mM extracellular (pipette) calcium. The excised patch was pretreated with α-chymotrypsin to destroy the exchanger regulatory processes. Substitution of cesium for 60 or 100 mM sodium in the bath solution was used to activatethe exchange current, as indicated. With 50 μm pipette movements, voltage changes detected by the calcium-selective electrode (Ca^{2+}-ISE) were 1.8, 0.2, and 0.7 mV in 4.4, 32, and 14 μM background $[Ca^{2+}]_i$, respectively. The calculated changes in $[Ca^{2+}]_i$ with these voltage values are 0.70, 0.53, and 0.83 μM, respectively. Therefore, the density of calcium fluxes are 0.13, 0.13, and 0.12 μM/pA at 4.4, 32, and 14 μM background $[Ca^{2+}]_i$, respectively. Upon changing cytoplasmic solutions, the voltage signals were adjusted to the same baseline, given as dotted lines in the voltage records. Thus, each dotted line indicates the background-free calcium given below the current trace. All of the scale bars given with the voltage signals indicate 0.7 μM $[Ca^{2+}]_i$ changes.

For the 30 pA current recorded, the accumulation amounts to 0.20 μM/pA, 58% larger than for results in Fig. 9 and quite close to the 0.25 μM/pA expected for 3Na/1Ca exchange process. We are frankly not certain what the causes of this variability might be, but possibilities to improve the accuracy of measurements will be discussed.

Extracellular Measurements: Valinomycin-mediated K-fluxes and their Calibration

To initiate potassium measurements from the extracellular (pipette) side, we chose to induce large transmembrane potassium fluxes by applying valinomycin (Eisenman et al., 1973) to patches in the presence of 120 mM cytoplasmic potassium and 0.5 mM extracellu-

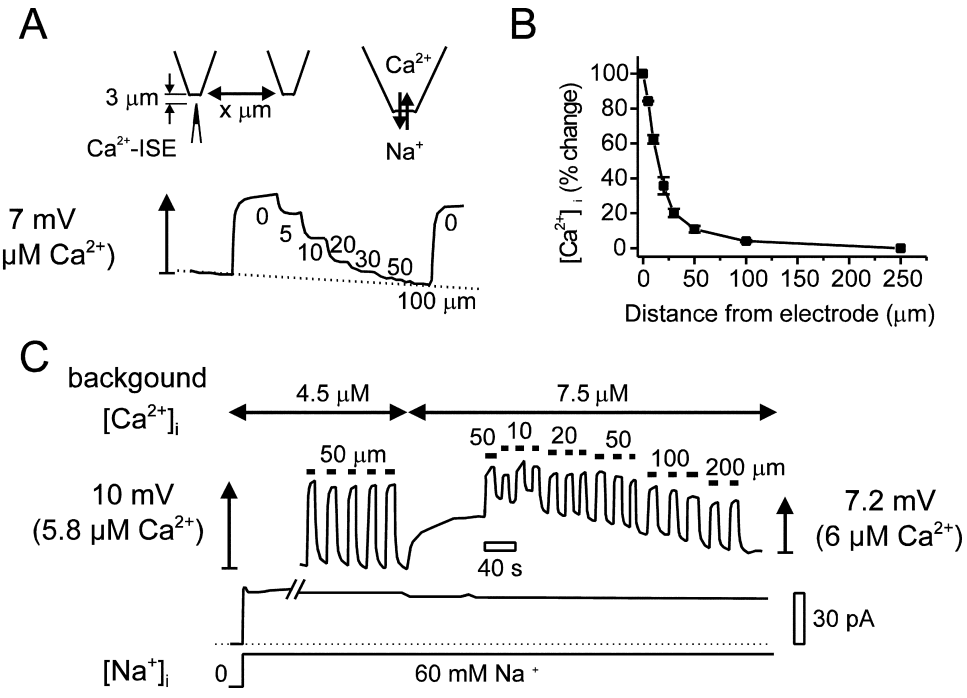

FIGURE 10. Spatial profile of the calcium diffusion in the bath solution. (A) Reverse Na/Ca exchange current was activated by 60 mM $[Na^+]_i$ in α-chymotrypsin–treated membrane patches. The patch pipette was moved to variable distances from the calcium-electrode in the z-axis (see upper diagram). Distances (μm) of the center patch pipette axis from the electrode tip are given with the voltage traces. Background free $[Ca^{2+}]_i$ is 7.5 μM, and the outward exchange current is 25 pA (current trace not depicted). (B) Summary of results from seven patches. The $[Ca^{2+}]_i$ changes are normalized and plotted against the distance from the electrode tip. (C) Outward exchange current was activated by 60 mM $[Na^+]_i$ and the calcium gradients were measured with 4.5 and 7.5 μM background $[Ca^{2+}]_I$, as indicated. The inner diameter of the pipette was 15 μm, and 3 mM calcium was included in the pipette solution.

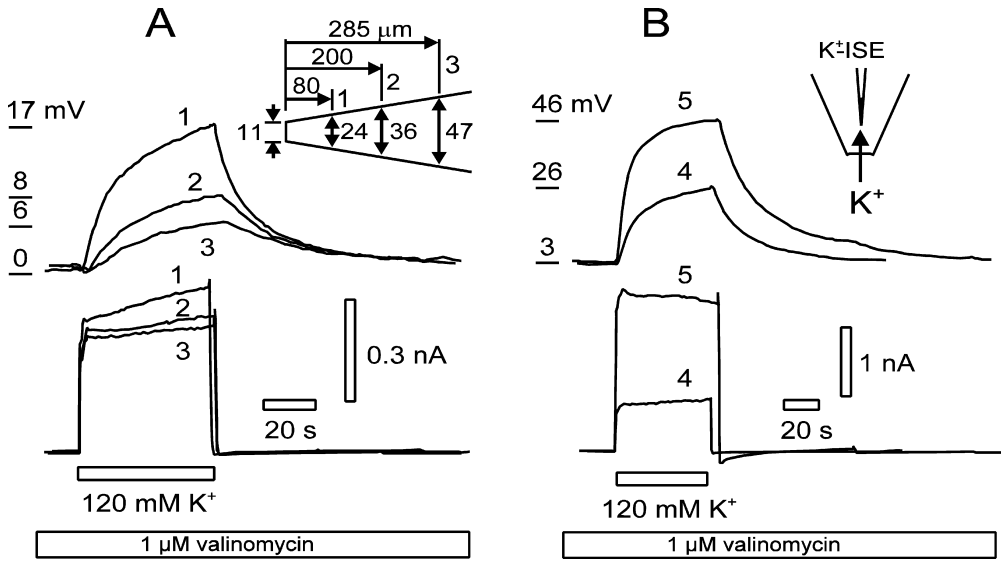

FIGURE 11. Measurement of potassium fluxes by intrapipette (extracellular) potassium–selective electrodes. Outward potassium current was activated by superfusing the patch with 120 mM potassium in exchange for NMG in the presence of 1 μM valinomycin. The potassium concentration in the pipette solution ($[K^+]_o$) was measured by a potassium-selective electrode (K^+-ISE). (A) $[K^+]_o$ was measured at 80 (trace 1), 200 (trace 2), and 285 μm (trace 3) distance from the membrane. The amplitudes of the currents are increased during the recording due to the longer exposure of valinomycin. The current trace 1 increased from 380 to 470 pA, trace 2 increased from 345 to 380 pA, and trace 3 from 320 to 350 pA, respectively. Voltage changes recorded by K^+-ISE were 16, 7.5, and 4.75 mV for trace 1, 2, and 3, respectively. The measured dimension of the patch pipette is appeared at the upper right corner of the traces. (B) Relationship between the current amplitudes and the potassium-fluxes. Different amplitudes of valinomycin-induced potassium currents were activated and $[K^+]_o$ was measured at 80 μm distance from the membrane. Net voltage changes of 23 and 43 mV were obtained from 0.77 and 2.24 nA potassium current, respectively. Initial potassium concentration included in the pipette solution was 0.5 mM, but during the repeated recordings the concentration raised gradually by the accumulation of potassium inside of pipette. The results shown in A and B were recorded from the same patch and the calculated changes in $[K^+]_o$ are shown in Fig. 12.

lar (pipette) potassium. As described in MATERIALS AND METHODS, NMG (120 mM) was the major monovalent cation on both membrane sides. Fig. 11 shows typical results with a potassium ISE placed at three different positions within the patch pipette, and also with different current magnitudes monitored at a single position. The membrane intruded into the tip of the pipette by at most 8 μm. Valinomycin (1 μM) was first applied with 0.5 mM potassium on the cytoplasmic side, resulting in no detectable membrane current or voltage response of the potassium ISE placed inside the patch pipette (unpublished data). Thereafter, 120 mM NMG-Cl was replaced by 120 mM KCl on the cytoplasmic side, with continued application of the ionophore. The 120 mM NMG-Cl solution was reapplied after 60 s, and the solution changes were repeated multiple times. Fig. 11 A shows recordings at the three different positions (80, 200, and 285 μm from the mouth of the patch pipette), typical for four similar experiments. Between responses, the electrode was repositioned, and the position was carefully calibrated.

As shown in Fig. 11 A, in the presence of valinomycin, the cytoplasmic application of 120 mM KCl induced large outward currents (~0.4 nA in the lower records of Fig. 11) that usually increased by 5–10% during the KCl application. Upon removing KCl, the currents returned to baseline immediately. The potassium ISE responses start with delays of ~2 to ~4 s when measured at 200 and 285 μm, respectively. The responses grow toward, but do not reach, a steady-state over the 60 s during which potassium was applied, ~16 mV at 80 μm, 7.5 mV at 200 μm, and 4.75 mV at 285 μm. The ISE responses return toward baseline with a time constant of 40 s after removing KCl. The declining phase of signals shows small delays at the positions farthest from the mouth of the pipette.

Fig. 11 B shows results for the larger potassium currents induced by higher valinomycin concentrations (3 and 10 μM) at the 80-μm electrode position from the mouth of the pipette. In these cases, the KCl solution was applied for only 50 s, but the electrode responses are increased to 23 and 43 mV, respectively. After completing these measurements, the patch pipette dimensions, illustrated in the inset to Fig. 11 A, were carefully determined under a microscope. Also, the potassium ISE was calibrated again to test that ISE function was stable.

Fig. 12 presents our analysis of the results described in Fig. 11. In brief, ion flux magnitudes were derived from the ISE responses by multiple routines, all of which underestimated the fluxes in relation to the measured potassium current magnitudes. Fig. 12 A shows the measured electrode dimensions (closed circles) and the best fits of a cone section (dotted lines) and of Eq. 10 (solid lines) to the dimensions. Fig. 12 B lists the five conditions analyzed and the mean current magnitudes used for analysis. From the electrode recordings presented in Fig. 11, the actual potassium concentra-

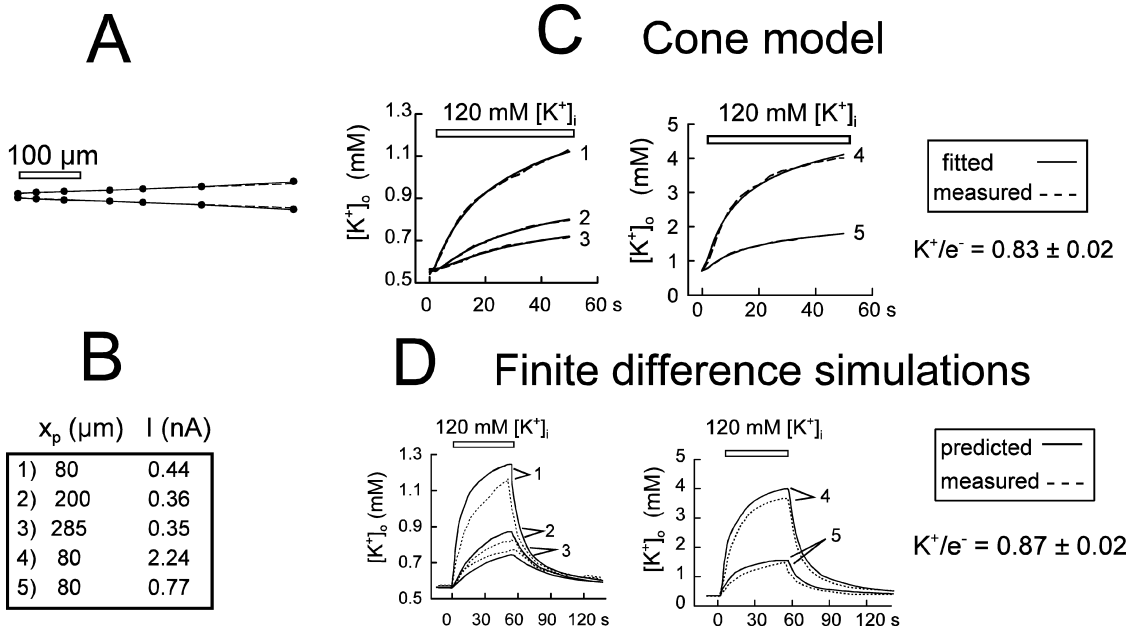

FIGURE 12. Analysis of valinomycin-induced extracellular (pipette) potassium accumulation. (A) Dimensions of the patch pipette used in the experiment described in Fig. 11 (circles) are recreated with very good accuracy by the best-fit of Eq. 10 to the dimensions (solid lines). The best fit to a simple cone (dotted lines) was used predict ion accumulation results using the analytical equation system (Eqs. 5–8). (C) Measured (dotted lines) and predicted experimental results (solid lines) using the analytical equation system with a diffusion coefficient of 2.03×10^{-5} cm^2/s and other parameters given in the text. Two parameters have been fitted by the least squares method, so that the accuracy of the time courses can be precisely evaluated, a baseline potassium concentration a scaler variable that quantifies the predicted ion flux per charge ratio (K^+/e^-). The average flux coupling value (K^+/e^-) for the five results is 0.83, indicating that the ion flux calculated from the ISE results is 17% smaller than expected from the potassium current magnitudes. (D) Finite difference simulations (solid lines) of experimental results (dotted lines) using best fit of the pipette dimensions, average current magnitudes from (B), and a potassium diffusion coefficient of 2.03×10^{-5} cm^2/s. The average flux per charge ratio (K^+/e^-) is 0.87 for the five results.

tions occurring in the pipette tip were calculated under the five conditions, and the concentrations are plotted in Fig. 12, C and D, as dotted lines with the numbering of results used in Fig. 12 B. Fig. 12 C presents the results from the analytical equations (Eqs. 5–8) for potassium accumulation (solid lines), which illustrate the accurate prediction of time courses using the same potassium diffusion constant used in Figs. 6 and 7 (2.04×10^{-5} cm^2/s). The half-angle of the pipette tip, $\theta_{1/2}$, is 3.8°, and the tip radius is 5.5 µm. A scaler variable was used to fit the predicted results to the experimental results by the least squares method. The average scaler value is 0.83 ± 0.02 for the five results, which indicates that the concentration changes are on average 17% smaller than predicted by the cone model. Clearly, the time courses of ion accumulation are very well predicted. In a separate data fitting routine (not depicted), the diffusion coefficient was also varied by the least-squares method to obtain the best possible description of each concentration response. The average value was $1.95 \pm 0.4 \times 10^{-5}$ cm^2/s, very close to the diffusion constant assumed in simulation.

Fig. 12 D shows the corresponding finite difference simulations (solid lines) with no scaling adjustments. The time courses of both the potassium accumulation and decline are very well predicted. The magnitudes of the potassium transients are systematically smaller than predicted by the simulations. On average, the measured results are 13 ± 2% less than predicted, a somewhat smaller discrepancy than predicted from the cone model. As expected from the fact that the responses do not reach a clear steady-state in 60 s, the discrepancy between predicted concentrations and measured concentrations was still larger when Eq. 2 was used to predict the steady-state concentration changes (24 ± 10.5% discrepancy). Using Eq. 4 to calculate the flux from the difference between concentrations at two positions along the pipette (i.e., 1 versus 2, 2 versus 3, and 1 versus 3 in Fig. 11), the average estimated ion flux was 15% smaller than expected from the current magnitudes. In our experience in eight similar experiments, the potassium concentrations predicted by simulations were never achieved during activation of valinomycin-mediated potassium currents. The largest discrepancies were 28%, and the smallest were 12%. Thus, it seems certain that some factor leads to systematic underestimation of potassium fluxes with the methods and analyses employed.

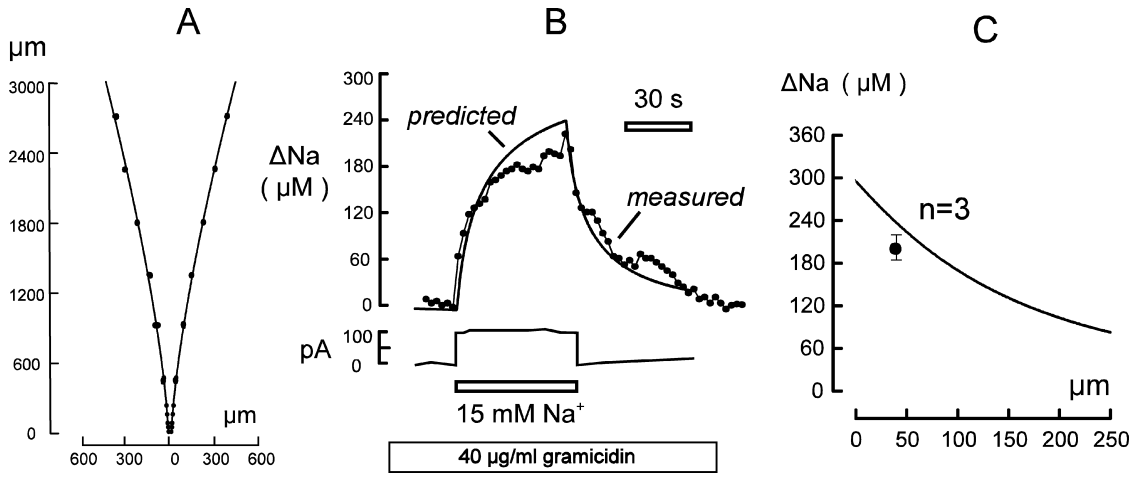

FIGURE 13. Measurement of sodium fluxes by intrapipette sodium–selective electrodes. (A) Dimensions of the patch pipette used in the experiment are recreated with very good accuracy by the best-fit of Eq. 10 to the dimensions (solid lines). (B) Outward sodium current (90 pA) was activated by superfusing the patch with 15 mM Na-gluconate in the presence of 40 µg/ml gramicidin. The lower record is the current response. The upper two records show the change of sodium concentration above baseline (2 mM, dotted record), calculated from the ISE responses, and the finite difference simulation for a 90 pA sodium current (solid record) using the pipette dimensions from (A) and other parameters given in the text. (C) The predicted steady-state sodium gradient in the pipette and the average sodium increment determined from three measurements using the same patch (± SEM).

Extracellular Measurements: Gramicidin- and Na/K Pump-mediated Na Fluxes and their Calibration

Next, we used gramicidin to induce relatively large outward sodium currents in giant cardiac patches and monitor sodium concentration changes in the pipette with sodium-ISEs. Fig. 13 shows an example, representative of four similar measurements, in which NMG-Cl is used as the only cation except sodium on both membrane sides. The pipette and the bath solutions contain 2.0 mM sodium at the start of the experiment. Fig. 13 A shows the pipette dimensions (data points) and the best description of the dimensions (solid lines) obtained by fitting Eq. 10 to the data points. In six experiments, 40 µg/ml gramicidin was applied in the presence of the low sodium cytoplasmic solution. Then, a cytoplasmic solution with 15 mM additional Na-gluconate was added to induce sodium flux, and typical current and concentration changes are shown in Fig. 13 B. The lower record is the current record during application of sodium in the continuous presence of 40 µg/ml gramicidin. Since neither chloride or gluconate permeates gramicidin channels (Cass and Dalmark, 1979), the outward current must be carried by sodium under these selected conditions. The upper records in Fig. 13 B give the concentration changes above baseline (2.0 mM), calculated from the sodium-ISE responses (dotted line), together with the concentration change predicted by finite difference simulation (solid line). The ISE tip was located 48 µM from the mouth of the patch pipette, and the simulation was performed with the fitted pipette dimensions shown in Fig. 13 A, a sodium current of 90 pA, and a sodium diffusion coefficient of 1.4×10^{-5} cm^2/s. The simulation predicts very accurately the time courses of concentration changes, but the magnitude of the concentration change is again underestimated, albeit less severely than for valinomycin-mediated potassium currents. Fig. 13 C shows the steady-state concentration profile predicted by the simulation (solid line) and the average concentration increment (± SEM) from three measurements in the same patch. From these, and the four additional repetitive measurements, we conclude that sodium fluxes are underestimated by ~10% using the sodium-ISEs and the simulation methods described.

Fig. 14 shows measurements of Na flux by Na/K pump activity in cardiac patches using an extracellular sodium ISE. Six similar measurements have been performed with similar results. The patch pipette was prepared to be nearly conical over a distance of 0.4 mm (average $\theta_{1/2}$, 3.8°), the pipette solution contained 120 mM NMG-Cl with 0.2 mM sodium and 5 mM potassium, and the ISE tip was located 53 µm from the mouth of the patch pipette. Fig. 14 A shows the membrane current and sodium-ISE responses when the Na/K pump was fully activated by applying 1 mM MgATP in the presence of 10 mM sodium on the cytoplasmic side. The three results shown, labeled 1–3, were recorded in the same patch over the course of 25 min. During this time, the pump current decreased considerably. For the 20 pA pump current, the Na electrode signal reaches 2 mV over 1 min, and the sodium electrode signals became smaller when the pump current decreased. The current magnitudes are plotted against

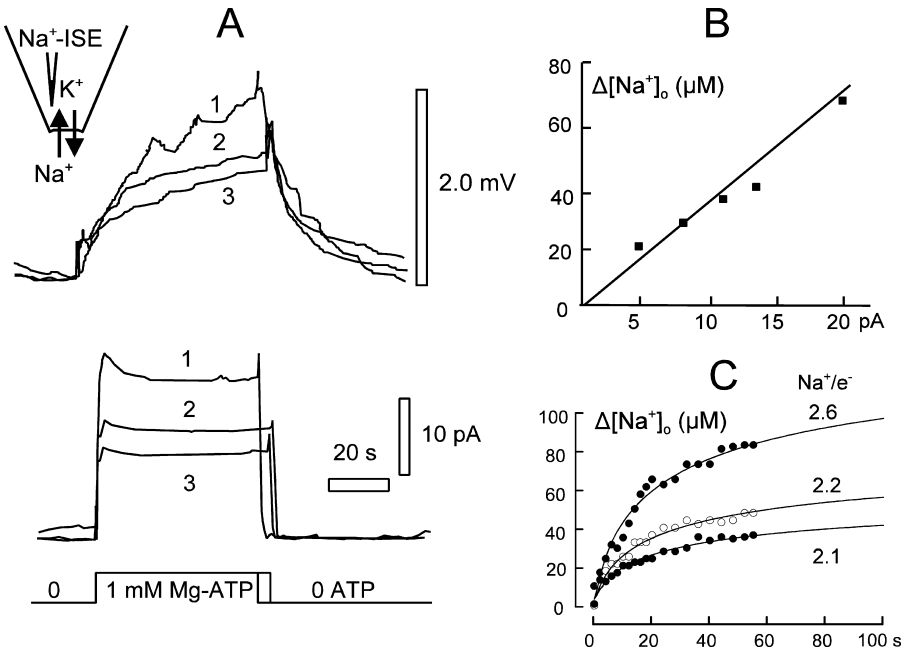

FIGURE 14. Measurement of Na/K pump-mediated sodium fluxes via an intrapipette sodium–selective electrode. (A) Outward Na/K pump current was activated by applying 1 mM MgATP, and the sodium concentration changes in the pipette ($[Na^+]_o$) were measured by the sodium-selective electrodes (Na^+-ISE). In this patch, pump activity showed run-down so that different amplitudes of the currents could be measured with the same ionic conditions. The relationship between current amplitudes and sodium concentrations are plotted in B. (C) Results from the cone section diffusion model (solid lines) and the finite difference simulations (not depicted) were fitted to experimental results by a scaler variable, and the average flux-coupling ratios are 2.6, 2.2, and 2.1 sodium ions per charge, as indicated.

the sodium concentration changes at 60 s in Fig. 14 B, and the points fall reasonably well on a straight line, as expected.

The electrode responses in Fig. 14 A were converted to concentration changes, and Fig. 14 C shows the least squares fits of the cone model equations to the experimental results. For each record, a flux coupling ratio (i.e., a scaler for each pump current) was treated as a free variable. The sodium diffusion coefficient was 1.4×10^{-5} cm^2/s. The fitted (solid) curves show no systematic deviation from the data, and the same diffusion coefficient predicted very well the time course of gradient dissipation using discrete simulation (unpublished data). The average scaling of results for the cone model and the finite difference simulations gave coupling ratios of 2.6, 2.2, and 2.1 sodium ions per charge, as indicated in the figure. In four of the five other measurements, the sodium to charge coupling was less than the expected value of three for a 3Na/2K pump stoichiometry. If one assumes that our calibration by simulations systematically underestimates sodium fluxes by 10%, as suggested by results with gramicidin (Fig. 13), the largest coupling ratio calculated (2.86) is still less than the three sodium per charge expected for perfect 3Na/2K stoichiometry.

Initial Tests for Electroneutral Ion Fluxes in Giant Cardiac Patches

As indicated in the INTRODUCTION, the methods developed in this article are intended to facilitate studies of electroneutral ion transporters. Therefore, after initiating and evaluating the sensitivity of ISE measurements, on both membrane sides, we attempted to identify activities of some of the major electroneutral ion transport systems thought to play important roles in the cardiac sarcolemma. These include Na/K/Cl cotransporters, calcium pumps, multiple bicarbonate transporters, and Na/H exchangers. However, we have failed up to now to detect reliably activities of these systems, probably for several different reasons, and we describe these initial efforts without figures.

For the bumetanide-sensitive Na/K/Cl cotransport system (Haas and Forbush, 1998), we attempted to monitor cytoplasmic potassium accumulation in the presence of extracellular sodium (150 mM), chloride (150 mM), and potassium (10 mM). Although this transport system is documented to mediate significant chloride and sodium influx in cardiac cells, we could detect no potassium flux to the cytoplasmic side under the conditions that optimized the thermodynamic driving force for Na/K/Cl cotransport. We estimate that a potassium flux equivalent to 15% of the flux mediated by the Na/K pump could have been resolved well. With the Na/K pump blocked (100 μM extracellular ouabain), we also tested whether a potassium flux could be activated in the presence of cytoplasmic ATP and commonly used inhibitor of the protein phosphatases, okadaic acid (0.1 μM). All results were negative.

In the nominal absence of extracellular calcium, the activation of forward Na/Ca exchange by 140 mM extracellular sodium and 20 μM cytoplasmic calcium results in very large signals at extracellular (intrapipette) calcium electrodes (>30 mV; unpublished data). In the absence of extracellular sodium, no extracellular calcium accumulation could be detected under conditions thought to optimize the operation of a sarcolem-

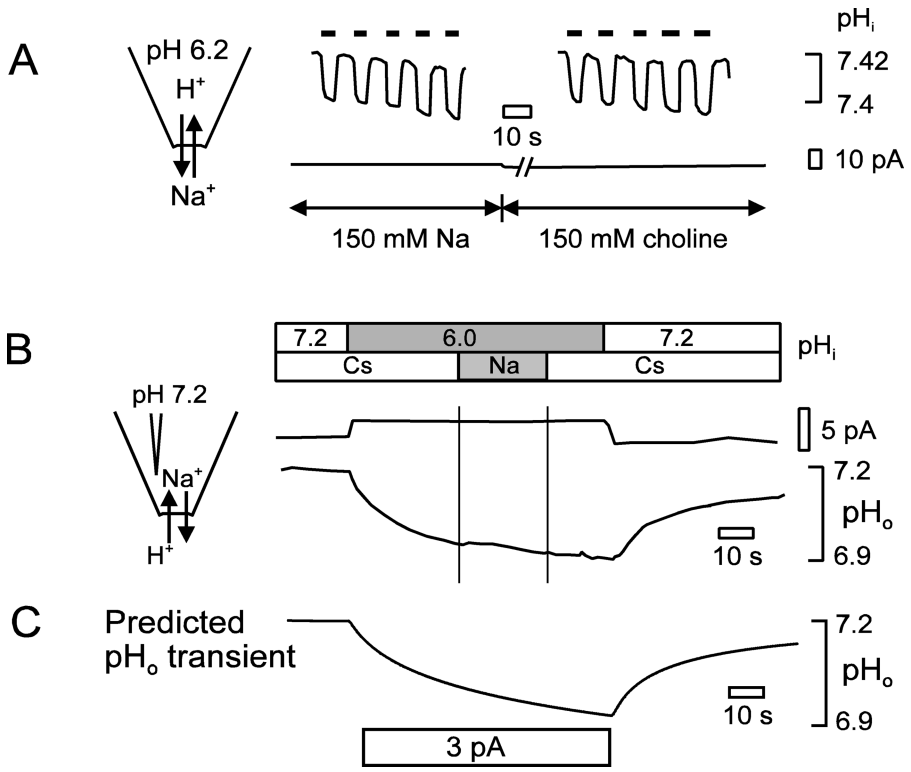

FIGURE 15. Measurement of proton fluxes induced by proton gradients in a giant cardiac membrane patch. (A) The pipette solution was sodium-free with a pH of 6.2. The patch pipette is oscillated in front of a proton ISE with a bath solution containing 0.05 mM TRIZMA and adjusted to 7.4. In presence of 150 mM sodium in bath solution, the proton-selective electrode records pH gradients of ~0.02 pH unit with 50 μm lateral movement of patch pipette from the electrode. Removal of cytoplasmic sodium does not change this gradient. A slight change of current reflects a smaller outward leak current carried by choline versus sodium. (B) Intrapipette pH recording. The experimental protocol is outline via the bar graph above the recordings. 140 mM sodium was included in the pipette solution with pH adjusted to 7.2 using 0.1 mM HEPES. The proton-selective electrode was placed 50 μm distance from the patch orifice. Superfusion of a cytoplasmic solution set to pH 6.0 results in an immediate outward current of 3 pA and a slowly developing acidification of the pipette tip by ~0.25 pH units over 90 s. Replacement of 120 mM cesium with 120 mM sodium on the cytoplasmic side does not affect the acidification. (C) Predicted pH_o changes for activation of a 3 pA proton current using discrete simulation of a pipette tip with the dimensions of the pipette employed in B. The pH is calculated assuming instantaneous equilibration of the 0.1 mM HEPES with protons and assuming a diffusion coefficient for HEPES of 0.7×10^{-5} cm^2/s.

mal calcium pump (2 mM cytoplasmic ATP, 0.2 μM calmodulin, 1 μM free calcium) (Carafoli, 1997; Guerini et al., 1998).

For bicarbonate transporters, we attempted to monitor biocarbonate transport indirectly via pH changes (i.e., alkalinization in association with bicarbonate accumulation). Since the giant patch is an open system, however, and the pK of the bicarbonate buffer system is 6.2, it is necessary to work at a very low pH to monitor bicarbonate transport via pH changes. As described subsequently, substantial proton fluxes are recorded in the giant patches when pH gradients are present, independent of bicarbonate, and for the time being these fluxes clearly complicate the indirect measurement of bicarbonate fluxes.

Na/H exchangers, when activated, are thought to mediate large proton and sodium fluxes in cardiac myocytes, large enough in pathological circumstances to overload the Na/K pump (Pierce and Meng, 1992; Karmazyn et al., 1999; Leem et al., 1999). Furthermore, large proton-dependent sodium fluxes have been identified in isolated cardiac vesicles under some conditions (Pierce and Philipson, 1985; Pierce and Meng, 1992; Goel et al., 2000, 2002). Although we optimized conditions to detect small proton fluxes, as described subsequently, we have not identified significant sodium-dependent proton flux under conditions that, on the basis of the literature to date, should favor a high Na/H exchange activity (150 mM extracellular sodium, cytoplasmic pH < 6.5, high cytoplasmic MgATP [5 mM], high cytoplasmic free calcium [2 μM], and high cytoplasmic calmodulin [0.2 μM] [Grinstein et al., 1983; Aharonovitz et al., 2000]). Presumably, additional signaling factors that activate cardiac Na/H exchangers are lost from the patches or are inoperative in patches. Results described in Fig. 15 document the sensitivity of our methods to monitor proton transport and the lack of a significant Na/H exchange-mediate proton flux in excised cardiac patches at 36°C.

Highly Sensitive Measurement of Proton Fluxes in Giant Membrane Patches

To establish conditions that should favor the proton influx mode of Na/H exchange, giant cardiac membrane patches were excised with pipettes containing choline (150 mM) as the major monovalent cation at pH 6.2. On the cytoplasmic membrane side, a minimal buffer concentration was employed (50 μM TRIZMA in Fig. 15, or 50 μM HEPES). As shown in the example in Fig. 15 A, an acidification was always detected on the cytoplasmic side of the patch with an inwardly directed pro-

ton gradient, here 0.02 pH units. When cytoplasmic sodium was replaced by choline there was a slight decrease in outward current, due to the lower conductance of choline through the patch leak pathway. However, replacement of sodium by choline had no detectable effect on the pH gradient. We mention that the solutions employed in these experiments were extensively equilibrated with nitrogen gas, and in these conditions the addition of a carbonic anhydrase, 0.2 mM acetazolamide, had no effect on the signals detected with proton-selective electrodes. Thus, the basal proton flux is not due to residual bicarbonate in the pipette solution with corresponding CO_2 diffusion out of the pipette.

As shown in Fig. 15 B, the reverse proton flux is also routinely observed when the pipette solution is buffered lightly with 100 μM HEPES at pH 7.2, and acidic solutions are applied to the cytoplasmic side. In this record, 150 mM sodium is present in the pipette solution, and the cytoplasmic solution initially contains 150 mM cesium as the sole monovalent cation. On acidification of the cytoplasmic solution from pH 7.2 to 6.0, the pH electrode that is placed 50 μm from the pipette tip detects a fall of pH to 6.9. The acidification develops slowly over the course of 1–2 min, and the substitution of 150 mM sodium for 150 mM cesium induces at most a very slight alkalinization on the pipette side. Upon switching back to pH 7.2 on the cytoplasmic side, the extracellular (pipette) pH returns nearly to baseline over 60 s.

Our analysis of the conditions of these experiments strongly suggests that proton fluxes equivalent to ≤1 pA transmembrane current would readily be detected. To our surprise, we routinely observed current changes in these experiments that are consistent with a genuine proton current, rather than an electroneutral ion–coupled flux, as the source of the proton fluxes observed in the absence of bicarbonate and carbon dioxide. As shown above the pH recordings in Fig. 15 B, the acidification on the cytoplasmic activates a 3 pA outward current, and similar currents were recorded with acidification using a variety of different solutions on both membrane sides (e.g., with cesium or choline or NMG as the major monovalent cation).

As illustrated via simulation in Fig. 15 C, the proton flux equivalent of the 3 pA current accounts very well for the observed extracellular acidification and the time courses of the pH changes. In this simulation, it is assumed that the HEPES buffer equilibrates instantly with protons, and that the diffusion constant of the buffer is the sole determinant of the time course of the signals. The diffusion constant of HEPES is assumed to be 0.7×10^{-5} cm^2/s and its dissociation constant (K_d) is assumed to be 3.2×10^{-8} M (Sigma-Aldrich). Thus, pH 7.2 corresponds to the presence of a total background proton concentration of 63 nM (H_0) in the presence of 100 μM HEPES buffer (B). The pipette dimensions in this experiment were the largest of all experiments presented (r_t = 12 μm and $\theta_{1/2}$ = 6.8°). Using the discrete simulation method, the free proton concentration (H_f) and the pH on the extracellular side at 50 μm from the pipette tip are simulated from the accumulation of protons (H_a) and the background proton concentration (H_0) using the steady-state solution for a single buffer system with α and β as temporary variables:

$$\alpha = K_d + B - (H_0 + H_a). \tag{14}$$

$$\beta = -(H_0 + Ha) \cdot K_d. \tag{15}$$

$$H_f = [-\alpha + \sqrt{\alpha^2 - 4 \cdot \beta}]/2. \tag{16}$$

$$pH = -\log(H_f). \tag{17}$$

DISCUSSION

The long-term goal of this work is to develop improved methods to analyze ion flux coupling of membrane transporters and to study the function and regulation of electroneutral ion transporters. With this perspective, our initial goal was to test whether ion gradients can be detected reliably next to giant membrane patches when ion transport is activated, and with what sensitivity. The measurements presented illustrate the detection of potassium, calcium, sodium, and proton gradients on both membrane sides of giant membrane patches. Microelectrodes have been used previously to detect ion gradients caused by water fluxes across artificial membranes (Saparov et al., 2000). Also, both ISEs and ion-sensing dyes have been used previously to detect transmembrane ion movements in intact tissues and cells in a noninvasive fashion (Nicholson, 1980; Hilgemann et al., 1983; Bers and MacLeod, 1986; Hilgemann, 1986; Smith et al., 1994; Arif et al., 1995; Smith, 1995), and most problems discussed in that work apply to the present work. Certainly, ion-sensitive fluorescent dyes that can be accurately calibrated could be used for many of the same applications, although the glass pipette tip is a very disadvantageous optical object. Beyond detection, our second goal was to quantify ion fluxes from the ion gradients detected and to assess the accuracy of the quantification. In the following, we review the success and limitations of the ISE methods to date, as well as the most important problems and surprises encountered in these initial measurements.

Technical and Theoretical Problems

The experiments described in this article combine for the first time ISE measurements with the giant patch recording. Most problems encountered could be solved

in a straight-forward fashion with adequate experimental experience. Flexible quartz capillary tubing can be used to prepare ISEs with the same success rates as obtained with standard glass pipettes, and the ISEs can then be positioned and manipulated easily within the giant patch pipette. Certainly, an automated method to reposition ISEs in the patch pipette would be advantageous. Nevertheless, no major experimental hurdles were experienced beyond those described previously with giant patches and pipette perfusion.

The accurate calibration of the ISE tip position with respect to the patch pipette mouth is critical for quantification of results, especially from the cytoplasmic side where ion gradients are steeper (Figs. 4 and 10) than inside the pipette tips with $<5°$ wall angles (Figs. 7 B and 11 A). Thus, good optics and multiple controls for placement of electrodes are essential. In this regard, careful pipette manipulation on the cytoplasmic side allows one to identify the peak ion accumulation in the plane perpendicular to the pipette axis, and the distance between the pipette tips in the third dimension can be quite accurately monitored when the pipettes are positioned at shallow angles with respect to the bottom of the recording chamber.

The principles of the ISE measurements and the optimization of experimental conditions are largely straight-forward. As described in the Figs. 3–7, the ion concentration changes induced by transport activity are dictated by diffusion, and the concentration changes and electrode responses are both readily predicted on both membrane sides when solution compositions are well controlled. For complete solution control in the pipette, it is sometimes important to avoid contamination with bath solution components during seal formation, and the most reliable approach is to use the intended pipette solution as the bath solution during seal formation. With these precautions, there are no obvious complexities in evaluating the ion flux magnitudes when diffusion coefficients are well established and ion buffering is not an issue. However, our best estimates of ion fluxes from simulations are typically 10–15% less than expected from current magnitudes and the assumption that conductances are selective under the conditions employed.

Experimental conditions for ion flux measurements are readily optimized from the consideration that the ISE signals are determined in first order by the ratio of the ion accumulation to the background ion concentration. Physiological concentrations of protons and calcium are in the nanomolar to micromolar range, and the background concentrations of protons and calcium can be determined accurately by using well-characterized buffers. Thus, the largest signals for a given ion flux magnitude can obviously be obtained for protons and calcium, when buffers are not employed or are employed at low concentrations. Of course, the presence of buffers introduces complexities in the calculation of fluxes, and buffer kinetics may become important. Therefore, our measurements of cytoplasmic calcium accumulation via Na/Ca exchange were made without buffers. For pH measurements with HEPES, we assume for now that buffer kinetics are very fast in relation to the diffusion times involved, namely several seconds.

Calibration and Interpretation of Ion Fluxes

For sodium and potassium, the responses of ISEs become "sub-Nernstian" at concentrations less than ~2.0 and 0.1 mM, respectively, and the loss of sensitivity at low concentrations dictated our choice of background potassium and sodium concentrations. The relatively high background concentrations decrease the relative sensitivity of potassium and sodium flux measurements many fold, but it is still clearly possible to detect and quantify ion fluxes generated by sodium pumps (Figs. 8 and 13). Electrode responses in the range of 1 to 2 mV are robust and reproducible, and with good certainty responses of 200–300 microvolts can be detected reliably. Thus, for the time being, the methods require that potassium and sodium fluxes constitute a significant fraction of the maximal Na/K pump flux to be detected reliable. From the cytoplasmic side, potassium flux to current ratios are calculated to be about twice greater for Na/K pump current than for a potassium current mediated by potassium channels. The results are close to expectations for a 3Na/2K coupling for the Na/K pump, and the absolute ion fluxes calculated for both potassium channel and pump activity were reasonably close to those expected.

Using diffusion models to calculate the sodium flux coupling for the Na/K pump, our highest estimate is that 2.6 sodium ions are moved for every charge moved (Fig. 14), or ~16% less than expected for a 3 Na/2K pump mechanism. However, our estimation of sodium flux mediated by gramicidin is ~10% less than expected for a selective ion current, and for the time being this suggests that the diffusion models underestimate ion flux. Thus, our best estimate of the maximum pump coupling is that 2.8 sodium ions move per charge transferred. This is very close to estimates from isotope flux measurements in squid giant axons (Rakowski et al., 1989). At this time, we have no reason to doubt that this discrepancy from a perfect 3 Na per charge is real, and the ISE methods should be useful to probe the physical basis for the discrepancy.

Our results for cytoplasmic measurements of calcium flux, mediated by Na/Ca exchange, show considerable variability. However, it is certainly impressive that the calculated calcium flux to current ratios are consistently less than expected for a 3Na/1Ca exchange pro-

cess (>10 measurements). We stress in this regard that the calibrations of the ISE were performed in the same solutions and over the same calcium concentration range as occur in the experiments (Figs. 9 and 10). Individual results were closer to those expected for a 4Na/1Ca stoichiometry than to a 3Na/1Ca stoichiometry. Clearly, the results are consistent with recent suggestions that the exchanger stoichiometry is not strictly 3-to-1 (Fujioka et al., 2000; Dong et al., 2002). As with the sodium pump, we conclude that the ISE methods have the capability to determine Na/Ca exchange flux coupling ratios, and that calcium flux per charge transfer is probably less than predicted by a perfect 3-to-1 stoichiometry. However, the variability of results requires further work to be confident about the details of flux coupling.

For the proton fluxes described in Fig. 15, our calculations of ion flux rest on two assumptions; first, that diffusion of protons is determined by the diffusion of their buffer (HEPES in Fig. 15), and second, that the buffer reaction occurs much faster than the diffusion of the buffer between the membrane to the tip of the ISE. With these assumptions, the acidification may be accounted for reasonably by assuming that the outward current recorded upon acidification is in fact a genuine proton current. This conclusion certainly requires rigorous testing, not least because specific proton currents (DeCoursey and Cherny, 2000; DeCoursey, 2000) have not been described in cardiac myocytes. An alternative is that the "leak" or seal pathway of the patch may allow relatively specific proton conduction, perhaps by a water-chain mechanism. From our experience over many years, we are confident that the leak pathway has a much higher conductance for monovalent cations than for divalent cations or for anions. A high proton conductance would therefore not be too surprising. Further experiments with other cell types, and tests for effects of proton channel inhibitors, should soon resolve this issue.

Why Are Ion Fluxes Underestimated with the ISE Method?

For potassium fluxes mediated by valinomycin, sodium fluxes mediated by gramicidin, and probably for sodium fluxes mediated by Na/K pump, the ISE methods underestimate ion fluxes, when they are calculated from diffusion models, by 10–15%. Smith et al. (1999), who initiated the use of ISEs in a self-referencing mode to assess ion fluxes from ion gradients, reported a similar discrepancy. In those experiments, ISEs were vibrated to detect ion gradients as quickly as possible, while still detecting the maximal signals that could be obtained at the different positions of the ISE. In short, the cause of the underestimation remains enigmatic. Possible explanations that we have eliminated include: (a) development of an electrical potential within the patch pipette tip, (b) systematic mistakes in the calibration of the ISEs, (c) systematic mistakes in the position of the ISE in the patch pipette, (d) mistakes in determining the dimensions of the patch pipette, and (e) mistakes in the diffusion constants employed in simulations. Three further possibilities that require careful testing are: (a) that the glass surfaces of the pipettes can modify the bulk diffusion of ions along the pipette tip, (b) that the presence of resin on the outer wall of the ISE leads to complexities in the diffusion of ions along pipette tip and/or the detection of ions along the outer surface of the electrode, and (c) that the presence of temperature gradients in the experimental chambers employed and along the pipette tip lead to complexities in the diffusion of ions along the pipette tip. Clearly, resolution of this issue is important for the further development and use of the ISE methods. For the time being, the best calibration method is probably the comparison of fluxes induced by transport with fluxes caused by ion-selective currents in the same membrane patch.

Perspectives for Electroneutral Transporters

Aside from the technical issues outlined above, our failure to identify activities of the Na/K/Cl cotransport and the Na/H exchange systems in excised giant cardiac patches is disappointing. For the Na/K/Cl cotransport system, it is well established that its activity depends on cell volume and protein kinase activities, probably involving a chloride-dependent regulatory pathway (Haas and Forbush, 1998). Obviously, most or all of the critical regulatory factors may be lost from excised patches. In the case of the Na/H exchange system, mostly NHE1 in cardiac myocytes, we have no clear lead as to what factor or factors may be most important (for review see Wakabayashi et al., 1997). Our preliminary experiments with the application of calmodulin, cytoplasmic calcium, GTPγS, PKC activators (phorbol esters or DAG), and hypoxic treatment of myocytes all failed to maintain exchange activity (unpublished data). Furthermore, negative results were obtained using excised patches from the M1 cell line (unpublished data), a kidney cortical collecting duct–derived cell line that has been shown to possess substantial NHE activity (Hill et al., 2002). Our experience with cardiac patches seems hard to reconcile with the described presence of a high Na/H exchange activity in isolated cardiac membrane vesicles, using low sodium concentrations to drive transport (Pierce and Philipson, 1985; Goel et al., 2000, 2002). For both Na/K/Cl cotransport and for Na/H exchange, it may be hoped that further experimentation with the methods described in the article will be a key to resolving open questions about transporter regulation.

In summary, the combination of ISE methods with giant patch methods described in this article seems promising for numerous future applications. As outlined in this DISCUSSION, great care must be taken to quantify ion fluxes accurately enough to determine ion flux coupling of transporters. At present, our calculations from diffusion models and direct calibrations by ion-selective currents are, at worst, 15% discrepant. Certainly, the limited selectivity of ISEs will limit some applications. But still, when conditions are selected carefully, the resolution of ion fluxes by ISEs can be very high. For protons, a flux equivalent to a 1 pA current can readily be resolved (Fig. 15). For calcium, fluxes equivalent to a 2 pA monovalent ion current can readily be resolved (Fig. 9). And for potassium and sodium, fluxes that constitute 15–20% of the maximal cardiac Na/K pump flux (i.e., equivalent to ~6 pA currents) would be resolved reliably (Figs. 8 and 14). Improved optics, automated ISE manipulation methods, and data averaging can very probably improve the accuracy of calibrations and allow the detection of smaller gradients.

We are very grateful to Luis Reuss (Galveston) for advice, encouragement, and the loan of an ISE amplifier; to Peter J. Smith and Mark Messerli (Woods Hole) for advice on preparing ISEs and for critical discussion of the manuscript; to Siyi Feng (UTSW) for expert technical assistance; to Art Peskoff (Los Angeles) for discussions of diffusion models; and to David C. Gadsby (New York) for careful criticisms of the manuscript.

This work was supported by Grant HL515323 to D.W. Hilgemann.

Olaf S. Andersen served as editor.

Submitted: 20 December 2002
Revised: 5 March 2003
Accepted: 11 March 2003

REFERENCES

Aharonovitz, O., H.C. Zaun, T. Balla, J.D. York, J. Orlowski, and S. Grinstein. 2000. Intracellular pH regulation by Na^+/H^+ exchange requires phosphatidylinositol 4,5-bisphosphate. *J. Cell Biol.* 150:213–224.

Arif, I., I.A. Newman, and N. Keenlyside. 1995. Proton flux measurement from tissues in buffered solution. *Plant. Cell Environment.* 18:1319–1324.

Apell, H.J., and S.J. Karlish. 2001. Functional properties of Na,K-ATPase, and their structural implications, as detected with biophysical techniques. *J. Membr. Biol.* 180:1–9.

Bers, D.M., and K.T. MacLeod. 1986. Cumulative depletions of extracellular calcium in rabbit ventricular muscle monitored with calcium-selective microelectrodes. *Circ. Res.* 58:769–782.

Bonen, A. 2001. The expression of lactate transporters (MCT1 and MCT4) in heart and muscle. *Eur. J. Appl. Physiol.* 86:6–11.

Boron, W.F. 2001. Sodium-coupled bicarbonate transporters. *JOP.* 2:176–181.

Carafoli, E. 1997. Plasma membrane calcium pump: structure, function and relationships. *Basic Res. Cardiol.* 92(Suppl 1):59–61.

Cass, A., and M. Dalmark. 1979. Chloride transport by self-exchange and by KCl salt diffusion in gramicidin-treated red blood cells. *Acta Physiol. Scand.* 107:193–203.

Collins, A., A.V. Somlyo, and D.W. Hilgemann. 1992. The giant cardiac membrane patch method: stimulation of outward Na^+-Ca^{2+} exchange current by MgATP. *J. Physiol.* 454:27–57.

De Weer, P., D.C. Gadsby, and R.F. Rakowski. 2001. Voltage dependence of the apparent affinity for external Na^+ of the backward-running sodium pump. *J. Gen. Physiol.* 117:315–328.

DeCoursey, T.E. 2000. Hypothesis: do voltage-gated H^+ channels in alveolar epithelial cells contribute to CO(2) elimination by the lung? *Am. J. Physiol. Cell Physiol.* 278:C1–C10.

DeCoursey, T.E., and V.V. Cherny. 2000. Common themes and problems of bioenergetics and voltage-gated proton channels. *Biochim. Biophys. Acta.* 1458:104–119.

Dong, H., J. Dunn, and J. Lytton. 2002. Stoichiometry of the cardiac Na^+/Ca^{2+} exchanger NCX1.1 measured in transfected HEK cells. *Biophys. J.* 82:1943–1952.

Eisenman, G., G. Szabo, S.G. McLaughlin, and S.M. Ciani. 1973. Molecular basis for the action of macrocyclic carriers on passive ionic translocation across lipid bilayer membranes. *J. Bioenerg.* 4:93–148.

Fujioka, Y., M. Komeda, and S. Matsuoka. 2000. Stoichiometry of Na^+-Ca^{2+} exchange in inside-out patches excised from guinea-pig ventricular myocytes. *J. Physiol.* 523:339–351.

Goel, D.P., T.G. Maddaford, and G.N. Pierce. 2002. Effects of omega-3 polyunsaturated fatty acids on cardiac sarcolemmal Na^+/H^+ exchange. *Am. J. Physiol. Heart Circ. Physiol.* 283:H1688–H1694.

Goel, D.P., A. Vecchini, V. Panagia, and G.N. Pierce. 2000. Altered cardiac Na^+/H^+ exchange in phospholipase D-treated sarcolemmal vesicles. *Am. J. Physiol. Heart Circ. Physiol.* 279:H1179–H1184.

Grinstein, S., C.A. Clarke, and A. Rothstein. 1983. Activation of Na^+/H^+ exchange in lymphocytes by osmotically induced volume changes and by cytoplasmic acidification. *J. Gen. Physiol.* 82: 619–638.

Guerini, D., E. Garcia-Martin, A. Zecca, F. Guidi, and E. Carafoli. 1998. The calcium pump of the plasma membrane: membrane targeting, calcium binding sites, tissue-specific isoform expression. *Acta Physiol. Scand. Suppl.* 643:265–273.

Haas, M., and B. Forbush, III. 2000. The Na-K-Cl cotransporter of secretory epithelia. *Annu. Rev. Physiol.* 62:515–534.

Haas, M., and B. Forbush, III. 1998. The Na-K-Cl cotransporters. *J. Bioenerg. Biomembr.* 30:161–172.

Hamill, O.P., A. Marty, E. Neher, B. Sakmann, and F.J. Sigworth. 1981. Improved patch-clamp techniques for high-resolution current recording from cells and cell-free membrane patches. *Pflugers Arch.* 391:85–100.

Hebert, S.C. 1998. Roles of Na-K-2Cl and Na-Cl cotransporters and ROMK potassium channels in urinary concentrating mechanism. *Am. J. Physiol.* 275:F325–F327.

Hilgemann, D.W. 1986. Extracellular calcium transients at single excitations in rabbit atrium measured with tetramethylmurexide. *J. Gen. Physiol.* 87:707–735.

Hilgemann, D.W. 1989. Giant excised cardiac sarcolemmal membrane patches: sodium and sodium-calcium exchange currents. *Pflugers Arch.* 415:247–249.

Hilgemann, D.W., M.J. Delay, and G.A. Langer. 1983. Activation-dependent cumulative depletions of extracellular free calcium in guinea pig atrium measured with antipyrylazo III and tetramethylmurexide. *Circ. Res.* 53:779–793.

Hilgemann, D.W., and C.C. Lu. 1998. Giant membrane patches: improvements and applications. *Methods Enzymol.* 293:267–280.

Hilgemann, D.W., and C.C. Lu. 1999. GAT1 (GABA:Na^+:Cl-) cotransport function. Database reconstruction with an alternating access model. *J. Gen. Physiol.* 114:459–475.

Hill, C., A.N. Giesberts, and S.J. White. 2002. Expression of isoforms of the Na^+/H^+ exchanger in M-1 mouse cortical collecting

duct cells. *Am. J. Physiol. Renal Physiol.* 282:F649–F654.
Hubner, C.A., V. Stein, I. Hermans-Borgmeyer, T. Meyer, K. Ballanyi, and T.J. Jentsch. 2001. Disruption of KCC2 reveals an essential role of K-Cl cotransport already in early synaptic inhibition. *Neuron.* 30:515–524.
Karmazyn, M. 2001. Therapeutic potential of Na-H exchange inhibitors for the treatment of heart failure. *Expert Opin. Investig. Drugs.* 10:835–843.
Karmazyn, M., X.T. Gan, R.A. Humphreys, H. Yoshida, and K. Kusumoto. 1999. The myocardial Na^+-H^+ exchange: structure, regulation, and its role in heart disease. *Circ. Res.* 85:777–786.
Kopito, R.R. 1990. Molecular biology of the anion exchanger gene family. *Int. Rev. Cytol.* 123:177–199.
Lauf, P.K., and N.C. Adragna. 2000. K-Cl cotransport: properties and molecular mechanism. *Cell. Physiol. Biochem.* 10:341–354.
Läuger, P. 1987. Dynamics of ion transport systems in membranes. *Physiol. Rev.* 67:1296–1331.
Leem, C.H., D. Lagadic-Gossmann, and R.D. Vaughan-Jones. 1999. Characterization of intracellular pH regulation in the guinea-pig ventricular myocyte. *J. Physiol.* 517:159–180.
Nicholson, C. 1980. Modulation of extracellular calcium and its functional implications. *Fed. Proc.* 39:1519–1523.
Pierce, G.N., and H. Meng. 1992. The role of sodium-proton exchange in ischemic/reperfusion injury in the heart. Na^+-H^+ exchange and ischemic heart disease. *Am. J. Cardiovasc. Pathol.* 4:91–102.
Pierce, G.N., and K.D. Philipson. 1985. Na^+-H^+ exchange in cardiac sarcolemmal vesicles. *Biochim. Biophys. Acta.* 818:109–116.
Press, W.H., B.P. Blannery, S.A. Teukolsky, and W.T. Vetterling. 1986. Numerical Recipes. Cambridge Press, Cambridge. 560–562.
Rakowski, R.F., D.C. Gadsby, and P. De Weer. 1989. Stoichiometry and voltage dependence of the sodium pump in voltage-clamped, internally dialyzed squid giant axon. *J. Gen. Physiol.* 93: 903–941.
Robinson, R.A., and R.H. Stokes. 1965. Electrolyte Solutions. Butterworths, London. 571 pp.
Russell, J.M. 2000. Sodium-potassium-chloride cotransport. *Physiol. Rev.* 80:211–276.
Saparov, S.M., Y.N. Antonenko, R.E. Koeppe, II, and P. Pohl. 2000. Desformylgramicidin: a model channel with an extremely high water permeability. *Biophys. J.* 79:2526–2534.
Sigworth, F.J. 1986. The patch clamp is more useful than anyone had expected. *Fed. Proc.* 45:2673–2677.
Smith, P.J. 1995. Non-invasive ion probes – tools for measuring transmembrane ion flux. *Nature.* 378:645–646.
Smith, P.J., K. Hammar, D.M. Porterfield, R.H. Sanger, and J.R. Trimarchi. 1999. Self-referencing, non-invasive, ion selective electrode for single cell detection of trans-plasma membrane calcium flux. *Microsc. Res. Tech.* 46:398–417.
Smith, P.J., R.H. Sanger, and L.F. Jaffe. 1994. The vibrating Ca^{2+} electrode: a new technique for detecting plasma membrane regions of Ca^{2+} influx and efflux. *Methods Cell Biol.* 40:115–134.
Smith, P.J., and J. Trimarchi. 2001. Noninvasive measurement of hydrogen and potassium ion flux from single cells and epithelial structures. *Am. J. Physiol. Cell Physiol.* 280:C1–C11.
Soleimani, M., and C.E. Burnham. 2001. Na^+:HCO^{3-} cotransporters (NBC): cloning and characterization. *J. Membr. Biol.* 183:71–84.
Stein, W.D. 1985. Transport and Diffusion across Cell Membranes. Academic Press, Inc., New York. 685 pp.
Wakabayashi, S., M. Shigekawa, and J. Pouyssegur. 1997. Molecular physiology of vertebrate Na^+/H^+ exchangers. *Physiol. Rev.* 77:51–74.